# SELF-CLEANING MEMBRANES BASED ON THERMORESPONSIVE DOUBLE NETWORK HYDROGELS

A Dissertation

by

RUOCHONG FEI

Submitted to the Office of Graduate Studies of
Texas A&M University
in partial fulfillment of the requirements for the degree of

DOCTOR OF PHILOSOPHY

| | |
|---|---|
| Chair of Committee, | Melissa A. Grunlan |
| Committee Members, | Gerard L. Coté |
| | Elizabeth Cosgriff-Hernandez |
| | Arum Han |
| Head of Department, | Gerard L. Coté |

December 2014

Major Subject: Biomedical Engineering

Copyright 2014 Ruochong Fei

ABSTRACT

By providing continuous glucose monitoring, a subcutaneously implanted glucose sensor would greatly improve the quality of life for diabetics. However, implantation of a sensor triggers the host response in which proteins and cells attach and accumulate onto the sensor membrane surface. This membrane biofouling severely limits sensor lifetime and accuracy by restricting glucose diffusion. Whereas attempts to reduce membrane biofouling have mostly relied on passivation approaches, we have designed "self-cleaning" membranes whose surfaces actively detach adhered proteins and cells upon thermal cycling. Thermoresponsive poly(*N*-isopropylacrylamide) (PNIPAAm) single network (SN) hydrogels deswell and reswell, respectively, when heated above and cooled below their volume phase transition temperature (VPTT). A self-cleaning PNIPAAm membrane would ideally be typically swollen (OFF-state) to facilitate glucose diffusion to the embedded sensor or sensing material. However, when transdermally heated above the VPTT, the membrane would reversibly switch to the deswollen state. This cyclical process would cause the active detachment of proteins and cells, thereby cleaning the surface to restore glucose diffusion. Double network (DN) designs, based on asymmetrically crosslinked, interpenetrating PNIPAAm networks, as well as considerations of membrane geometry and size were utilized to achieve the functional requirements of a self-cleaning membrane.

This research was comprised of four major studies. In the first study, thermoresponsive PNIPAAm DN nanocomposite hydrogels containing inorganic polysiloxane nanoparticles were prepared. Inorganic, hydrophobic polysiloxane

nanoparticles (~50 nm and ~200 nm average diameters) were introduced during formation of the 1st or 2nd network of the PNIPAAm DN hydrogel.

In the second study, thermoresponsive PNIPAAm DN hydrogels were prepared with an electrostatic comonomer (2-acrylamido-2-methylpropanesulfonic acid, AMPS). The negatively charged AMPS was incorporated at varying levels (0-75 wt% based on NIPAAm weight) during formation of the 1st network but was excluded from the 2nd network to retain the thermoresponsive behavior.

In the third study, the combined impact of a PNIPAAm DN design and reduction of hydrogel size to the micron-scale on thermosensitivity and cell release efficacy was evaluated. PNIPAAm SN and DN hydrogels were prepared as 1.5 mm-thick planar slabs as well as micropillar arrays.

The final aspect of this work was focused on evaluating the charged membrane design in terms of functional requirements essential to a final implanted glucose biosensor. This study paralleled previous efforts to likewise characterize a particular DN nanocomposite membrane.

# DEDICATION

To My Parents

This dissertation is dedicated to my parents for their love, encouragement and endless support.

# ACKNOWLEDGEMENTS

First of all, I would like to express my deepest gratitude to my advisor and committee chair, Prof. Melissa A. Grunlan, for her invaluable guidance, caring and patience. During the past five years, she has supported me not only by providing a research assistantship, but also academically and emotionally through the rough road to complete this dissertation. Her wisdom, knowledge and commitment to the highest standards inspired and motivated me.

Second, I would like to thank my committee members, Dr. Gerard L. Coté, Dr. Elizabeth Cosgriff-Hernandez, and Dr. Arum Han for their support throughout the course of this research. I appreciate your suggestions and input as well exposing me to diverse ideas and new ways of thinking.

Third, I would also like to thank all of my group members, for their support and the memories that we have shared in the lab.

Last but not least, I would like to thank my family. They have always been supporting and encouraging me with their best wishes.

TABLE OF CONTENTS

Page

LIST OF FIGURES

Page

LIST OF TABLES

Page

# CHAPTER I

# INTRODUCTION

## 1.1. Background

### *1.1.1. Diabetes challenge*

Diabetes mellitus is a growing worldwide public health problem. Affecting more than 180 million people worldwide, this number is estimated to almost double by 2030 [1, 2]. In the USA, over $245 billion dollars of direct medical costs were incurred to treat diabetics in 2012 [3]. For diabetics, the inability to regulate production or metabolism of insulin results in blood glucose concentration fluctuations above and below the normal range of 80 – 120 mg/dL. In addition to short-term complications, poorly controlled blood sugar levels frequently lead to serious long-term complications, including heart diseases, kidney failure, blindness, limb amputation, and even death [4, 5]. Close monitoring of blood glucose concentrations is widely recognized as a core component of effective diabetes management [6]. Currently, blood sugar levels are most commonly

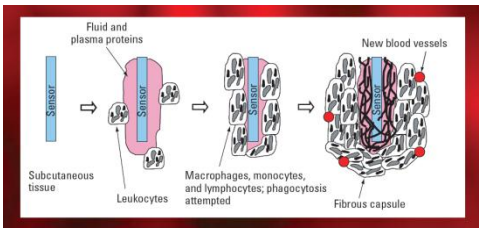


**Figure 1.1.** A subcutaneous glucose biosensor could provide convenient, continuous monitoring of glucose levels. However, biofouling prevents glucose diffusion and, hence, the sensor fails in only 3-7 days. A membrane that controls this process could make continuous glucose monitoring a reality [8].

monitored via a finger prick test.

Unfortunately, the finger-prick test is uncomfortable, inconvenient and, as a result, patient compliance (e.g. testing at least 4-6 times daily) is often not met. Furthermore, this monitoring method provides only intermittent "snap shots" of blood sugar levels. Because of this poor approach to monitoring blood sugar levels, diabetic patients are highly susceptible to serious short and long-term complications. Thus, an implanted continuous glucose monitoring (CGM) biosensor is a highly desirable alternative as it would provide constant knowledge of blood sugar levels, ultimately resulting in superior management of diabetes [7].

### *1.1.2. Limitations of current continuous glucose monitoring (CGM) systems*

Currently, only a few CGM devices have been approved by the FDA, but all are transdermal and none display a lifetime greater than 7 days. These CGMS (along with their lifetimes) include: (1) Medtronic MiniMed Guardian REAL-Time® (3 days), (2) Abbott FreeStyle Navigator Continuous Glucose Monitoring (CGM) Devices (5 days), and (3) the Dexcom SEVEN Plus (7 days). These CGM devices consist of a disposable transdermal sensor that measures the amount of glucose in the interstitial fluid, and an electronic hand-held receiver that reads the signal sent out from the sensor. However, the limited lifetime and physical irritation of transdermal CGMs have stunted their impact in the market. The limited lifetime of transdermal CGMs is primarily attributed to biofouling, which occurs as part of the foreign body response. Their limited lifetime and

need for frequent removal and replacement has also necessitated a transdermal rather than a more desirable fully subcutaneous design.

### *1.1.3. Membrane biofouling – a barrier to long-term functionality*

Membrane biofouling of subcutaneously (**Figure 1.1**) or transdermally implanted biosensor, is considered to be a leading cause of failure [8, 9]. When a sensor is implanted into the subcutaneous tissue, a cascade of events is initiated as part of the foreign body reaction [9-13]. As it progresses, glucose diffusion is increasingly compromised due to the accumulation of proteins and cells on the surface which decrease sensor accuracy and lifetime. At the beginning of the foreign body reaction, implantation of the sensor causes injury to the surrounding tissue, leading to the release of fluids, proteins and cells from the vasculature, also known as exudation. This process triggers the inflammatory response. During acute inflammation, neutrophils predominate but are replaced by monocyte-derived macrophages during chronic inflammation. Following inflammation, a healing response occurs which is marked by the formation of granulation tissue by fibroblasts and vascular endothelial cells. In addition, small blood vessels sprout from pre-existing vessels (i.e. angiogenesis). However, during the foreign body reaction, adherent macrophages can also fuse into foreign-body giant cells (FBGCs) which may persist for the lifetime of the implant. Fibrosis (i.e. fibrous encapsulation) ultimately surrounds the implant, isolating it from the tissue.

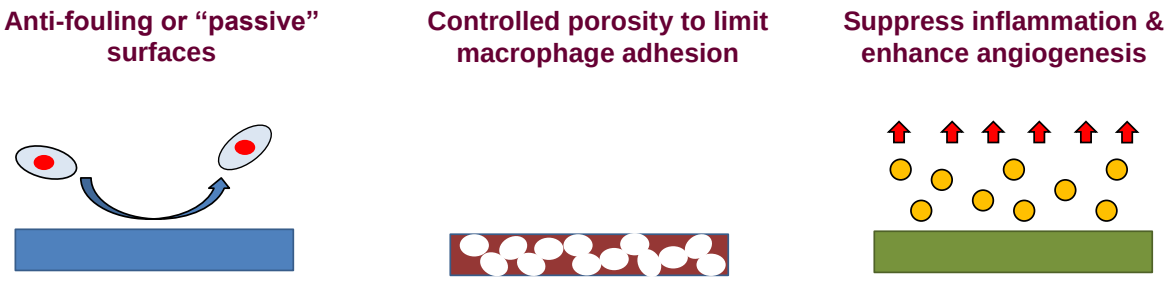


**Figure 1.2.** (A) Surface passivation. (B) Structure porosity. (C) Angiogenesis factor release.

*1.1.4. Current approaches to control membrane biofouling*

Reported approaches to control membrane biofouling are largely based on different passivation strategies. In this way, the membrane is designed to prevent or diminish the adhesion of proteins and cells (**Figure 1.2A**). Reported strategies to develop "anti-fouling" membrane materials include those based on poly(ethylene glycol) (PEG) [14] and zwitterions [15, 16]. In addition, topography (e.g. roughness, texture, and porosity) has been evaluated to enhance tissue in-growth and neovascularization while disrupting fibrosis (**Figure 1.2B**). Notably, porous membranes (5 – 60 μm diameter pores) have been prepared including those based on poly(tetrafluoroethylene)(PFTE) [17, 18], e-PTFE,[19] poly(vinylalcohol)(PVA) [20], poly(hydroxyl-ethylmethacrylate) (PHEMA) [21], and poly-L-lactic acid (PLLA) [22]. A third general passivation approach is to suppress inflammation and fibrosis as well as enhance angiogenesis around the sensor (**Figure 1.2C**). For instance, membranes that release nitric oxide [23, 24], dexamethasone [25] and vascular endothelial growth factor (VEGF) [26] have been studied.

## 1.2. Innovation

In contrast to passivation approaches, we sought to develop a membrane design that would actively control biofouling. This membrane is designed to actively "self-clean" through simple, readily controlled transdermal cyclical heating (**Figure 1.3**). Specifically, the membrane would undergo a cyclical, reversible transition from a swollen to deswollen state resulting in the release of adhered proteins and cells. While

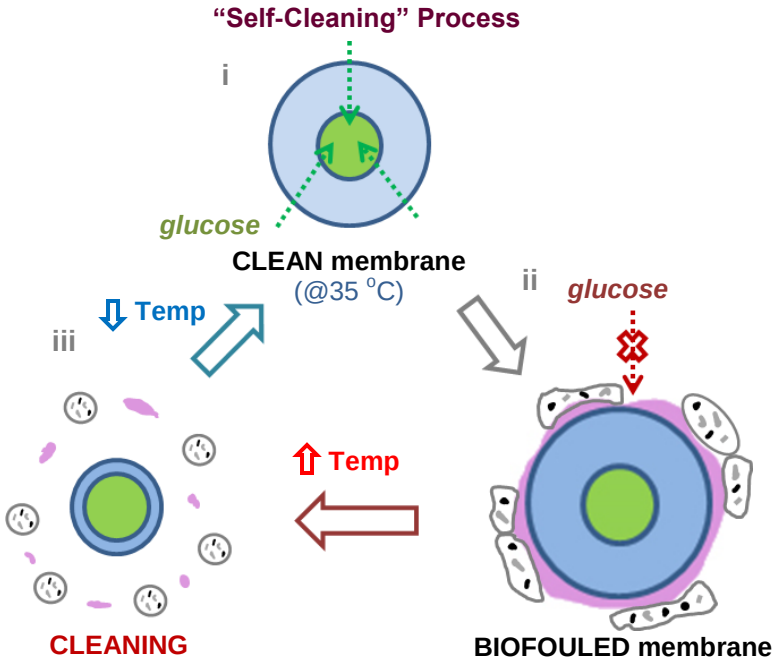


**Figure 1.3.** (i) At 35°C (i.e. body temperature of wrist subcutaneous tissue), the sensor membrane is in a swollen state ("OFF-state"). A swollen membrane will permit glucose diffusion and helps minimize cell adhesion (ii) Over time, proteins and cells accumulate on the membrane surface and begin to limit glucose diffusion. Conventional sensor membranes would require replacement of the sensor at this stage. (iii) Transdermal heating will invoke membrane deswelling, causing the release of proteins and cells ("ON-state").Cooling to body temperature returns the membrane to its swollen state.

thermal modulation of thermoresponsive hydrogels has been shown to effectively release adhered cells (including macrophages) *in vitro*, they have not been used likewise used *in vivo* [27-33].

### *1.2.1. Materials strategy*

Several functional requirements must be met by the self-cleaning membrane, including excellent thermosensitivity (i.e. fast deswelling/reswelling) and robust mechanical properties for insertion and removal of the membrane-enclosed sensor. Compared to conventional (i.e. single network, SN) hydrogels, double network (DN) hydrogels display enhanced mechanical properties as well as a high degree of swelling (i.e. hydration) [34-36]. DN hydrogels are comprised of two assymetrically crosslinked interpenetrated networks (IPN) where one network is more highly crosslinked than the other. While PNIPAAm IPNs have been previously reported,[37] PNIPAAm DN hydrogels have not. In this research, two thermoresponsive membrane designs were explored based on a DN design. The first is a PNIPAAm DN nanocomposite design containing polysiloxane nanoparticles (**Figure 1.4**). In previous work reported by our group [38], PNIPAAm SN nanocomposite hydrogels demonstrated enhanced thermosensitivity versus PNIPAAm SN hydrogels. Thus, the corresponding DN nanocomposites were expected to further improve thermosensitivity. In the second design, a series of PNIPAAm DN hydrogels containing an electrostatic comonomer (2-acrylamido-2-methyl-propanesulfonic acid, AMPS) were explored (**Figure 1.4**). The electrostatic repulsive forces between negatively charged AMPS molecules was

expected to improve the mechanical properties of the membrane while enhancing swelling and optical transparency.

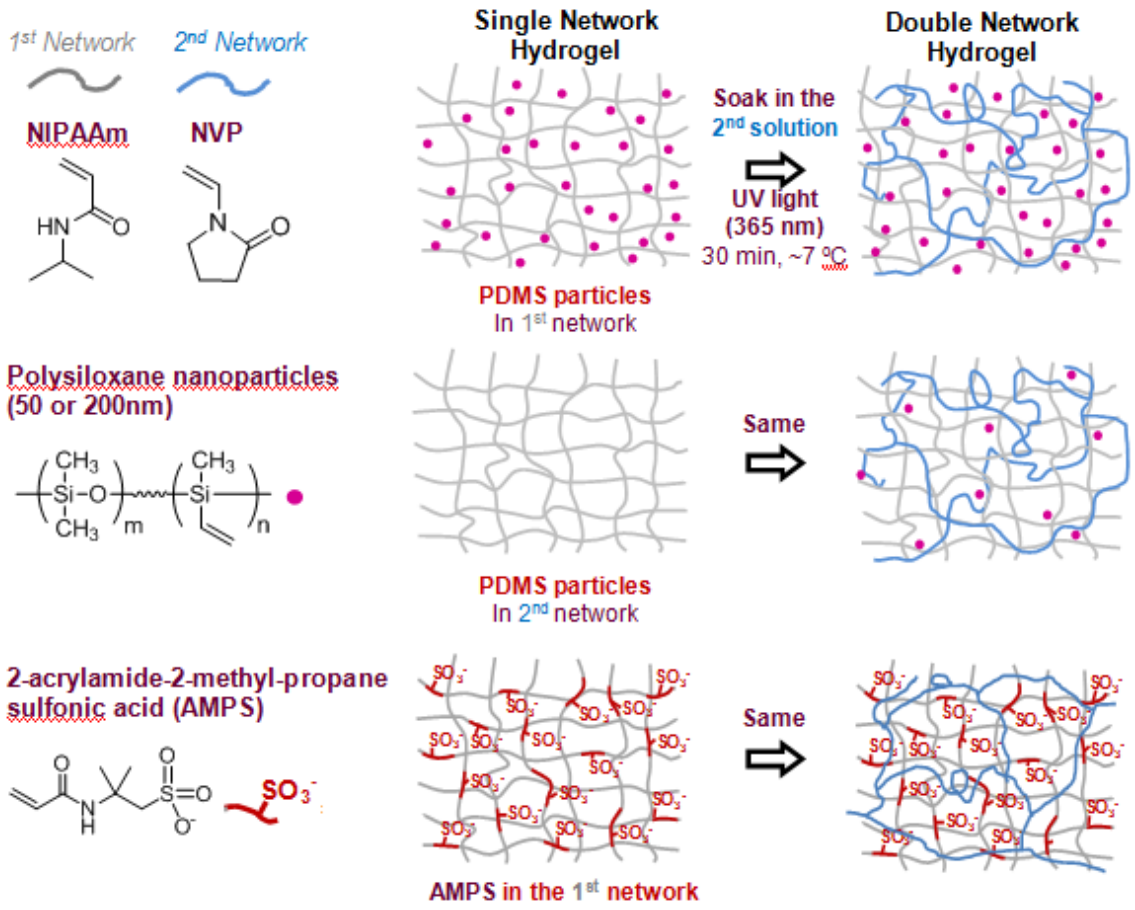


**Figure 1.4.** PNIPAAm DN hydrogel designs evaluated as self-cleaning membranes for implanted glucose biosensors.

*1.2.2. End use design*

In addition to membrane chemistry, the final membrane geometry was also considered. We envisioned that a cylindrical geometry would permit the ready insertion of the membrane-enclosed sensor into the subcutaneous tissue of the wrist via a tumor transducer needle. Such a cylindrical device may be also readily removed at the conclusion of the sensor lifetime. The cylindrical membrane could contain the sensor or sensing material either in the interior or central cavity or, alternatively, disperse throughout the membrane. A "watch-like device" or another such device worn over the implanted biosensor site would contain a heating component to invoke periodic, cyclical transdermal heating to affect self-cleaning of the membrane. Such a device could also contain, for instance, an optical transdermal probe for continuous glucose sensing. Thus, a diabetic having such a subcutaneously implanted biosensor would have convenient access to continuous glucose monitoring. This would represent a huge improvement to glucose monitoring versus the finger-prick test and even current transdermal CGMs.

## 1.3. Approach

*1.3.1. Rationale*

Thermal modulation reversibly switches crosslinked PNIPAAm-based hydrogels from a water-swollen, hydrophilic state to a deswollen, hydrophobic state [39, 40]. This process has been shown to effectively cause controlled detachment of cells (including macrophages) *in vitro* [27-33]. For the purpose of a subcutaneously implanted glucose biosensor membrane, the membrane would be swollen in the "OFF state", thereby

permitting adequate diffusion of glucose to the sensor or sensing materials. To control biofouling, the membrane would be heated transdermally to cause it to switch to the deswollen "ON state". The process of thermal cycling would cause the membrane to "self-clean" by eliciting protein and cell detachment. The utility of a PNIPAAm-based hydrogel as a self-cleaning membrane of an implanted glucose biosensor membrane demands three key functional requirements, including: (1) swollen in the "OFF-state" (i.e. swollen at body temperature of the subcutaneous tissue of wrist, 35 °C) for adequate glucose diffusion, (2) rapid thermal modulation to induce efficient release of adhered proteins and cells, and (3) robust mechanical properties for insertion, removal, and integrity while indwelling.

### *1.3.2. Strategy*

To achieve the functional requirements of the self-cleaning membrane, two PNIPAAm DN hydrogel designs were explored, including a nanocomposite design containing polysiloxane nanoparticles and a second design based on incorporation of an electrostatic comonomer, AMPS (**Figure 1.4**). Considerations of the membrane cylindrical geometry were also made, including in terms of glucose diffusion and cell release behavior. PNIPAAm DN hydrogels were prepared by increasing the amount of crosslinker in the 1$^{st}$ network relative to the 2$^{nd}$ network. For both designs, such that the implanted membranes would be theoretically swollen in the "OFF-state", it was verified that the VPTT of the membrane could be raised from ~33 $^{\circ}$C (i.e. that of pure PNIPAAm SN hydrogels) to ~38-39 °C (i.e. above 35 °C or the body temperature of the

subcutaneous body tissue of the wrist). This was accomplished by the inclusion of a small amount of a hydrophilic co-monomer, *N*-(vinylpyrrolidone) (NVP) (~2 wt% based on NIPAAm). For the PNIPAAm DN nanocomposite design, polysiloxane nanoparticles of two different diameters (~50 and 200 μm) were incorporated during the formation of either the 1st or 2nd network. In the case of the electrostatic PNIPAAm-*co*-AMPS DN design, AMPS was incorporated at varying levels (0-75 wt% based on NIPAAm weight) during formation of the 1st network in order to maintain thermosensitivity. For both designs, the impact of membrane composition was systematically studied for planar membranes with the appropriate methods, including: VPTT (by differential scanning calorimetry, DSC), thermosensitivity (by gravimetric deswelling/reswelling experiments), morphology (by scanning electron microscopy, SEM), modulus and strength (by quasi-static tensile and/or compression tests) and storage modulus (by dynamic mechanical analysis, DMA). The impact of a cylindrical micropillar geometry versus a planar, mm-thick geometry were made by preparing micropatterned PNIPAAm SN and DN hydrogels (~200 μm diameter). Comparison of thermosensitivity and self-cleaning ability was made by evaluating temperature-driven changes in pillar diameter and cell-release, respectively. Finally, membrane designs were considered in more specific terms related to their ability to function as a self-cleaning membrane for an implanted glucose biosensor. This included measurement of glucose diffusion and modeling of glucose diffusion lag time for membranes whose VPTT was adjusted to ~38 °C with NVP. In addition, thermally-driven deswelling/reswelling and cell release from cylinders with dimensions expected for implantation (1.5 x 5 mm) was evaluated. For

the DN nanocomposite design, these characteristics were previously reported [41]. In this work, we extend this analysis to the electrostatic DN design.

# CHAPTER II

# THERMORESPONSIVE NANOCOMPOSITE DOUBLE NETWORK HYDROGELS*

## 2.1. Overview

The utility and efficacy of thermoresponsive poly(*N*-isopropylacrylamide) (PNIPAAm) hydrogels as smart materials is limited by their physical properties. In this study, we sought to design PNIPAAm nanocomposite hydrogels which displayed enhanced mechanical properties as well as deswelling/reswelling kinetics but without reducing equilibrium swelling or altering the convenient volume phase transition temperature (VPTT) of PNIPAAm. PNIPAAm hydrogels were formed as double networks (DN) comprised of a tightly crosslinked 1$^{st}$ network and a loosely crosslinked 2$^{nd}$ network. In addition, polysiloxane nanoparticles of two different average diameters (~50 nm and ~200 nm) were incorporated during formation of the 1$^{st}$ or 2$^{nd}$ network. The influence of the hydrogel composition on VPTT, morphology, equilibrium swelling, deswelling/reswelling kinetics and mechanical properties was evaluated. We observed that DN hydrogels formed with ~200 nm polysiloxane nanoparticles introduced during formation of the 1$^{st}$ network achieved the best combination of the desired properties.

* Reprinted with permission from "Thermoresponsive nanocomposite double network hydrogels" by Fei R, George JT, Park J, Grunlan MA, 2012. *Soft Matter*, 8, 481-7, Copyright 2014 by the Royal Society of Chemistry.

## 2.2. Introduction

Thermal modulation reversibly switches crosslinked poly(*N*-isopropylacrylamide) (PNIPAAm) hydrogels between a water-swollen, hydrophilic state and a deswollen, hydrophobic state [39, 42]. A volume phase transition temperature (VPTT) of ~33-35 °C makes PNIPAAm hydrogels particularly useful to prepare "smart" materials for biological applications [43-46]. These applications include microfluidic actuation [47-50], separation [47, 51, 52], controlled drug delivery [47, 53-55] and controlled detachment of adsorbed cells and proteins for cell sheet tissue engineering [29, 47, 56], anti-fouling coatings [57-59], and "self-cleaning" membranes for implanted biosensors [60-63].

In these applications, conventional PNIPAAm hydrogels prepared via copolymerization of *N*-isopropylacrylamide (NIPAAm) and a crosslinker such as *N*,*N*'-methylenebisacrylamide (BIS) have limited efficacy due to poor mechanical properties as well as slow deswelling/reswelling kinetics (i.e. thermosensitivity) [64]. It is typical to employ strategies which reduce equilibrium swelling in order to improve hydrogel mechanical properties such as increasing crosslink density [65, 66] and introducing discrete fillers [67]. However, a highly swollen state is critical for certain applications involving transport or separation. In addition, many strategies useful to enhance the thermosensitivity of PNIPAAm hydrogels (without altering the VPTT) diminish mechanical properties, including: comb-type networks,[68-70] heterogeneous morphologies [71-73], poration [74-77] or open channel structures [78].

Nanocomposite hydrogels, including those based on PNIPAAm, have attracted recent attention, particularly for biological applications [79, 80]. PNIPAAm-based nanocomposite hydrogels have been prepared with various fillers such as iron oxide nanoparticles [81], gold nanoparticles [82], silicate nanoplatelets [83, 84], grapheme [85, 86], carbon nanotubes [87] and silica [88]. We recently reported PNIPAAm nanocomposite hydrogels prepared by introduction of hydrophobic polysiloxane nanoparticles with average diameters of ~50 nm [89] and ~200 nm [38]. Without changing the VPTT, the polysiloxane nanoparticles produced an increase in hydrogel rigidity. However, this was at least due in part to a decrease in equilibrium swelling of the nanocomposite hydrogels. Notably, we also observed that nanocomposite hydrogels containing ~50 nm particles exhibited an exceptionally enhanced rate of deswelling [90].

In this study, we sought to design a PNIPAAm nanocomposite hydrogel which displayed enhanced mechanical properties as well as deswelling/reswelling kinetics and without reducing equilibrium swelling or altering the VPTT. Compared to conventional or single network (SN) hydrogels, double network (DN) network hydrogels are associated with enhanced mechanical properties as well as a high degree of swelling [35, 90]. DN hydrogels are a class of interpenetrating polymer networks (IPNs) comprised of two highly asymmetrically crosslinked networks. Gong and co-workers reported the first DN hydrogels consisting of tightly crosslinked, ionizable 1$^{st}$ network comprised of poly(2-acrylamide-2-methyl-propane sulfonic acid) (PAMPS) and sparsely crosslinked, neutral 2$^{nd}$ network comprised of poly(acrylamide) (PAAm) [91, 92]. DN hydrogels consisting for poly(ethylene oxide) (PEO) and poly(acrylic acid) (PAA) have also been

prepared which are essentially the inverse of those prepared by Gong et al [93]. These are comprised of a tightly crosslinked, neutral 1st network of PEO and a loosely crosslinked, ionizable 2nd network of PAA. Several other DN hydrogels have been reported but a similarly non-thermoresponsive [94, 95]. While Zhang et al. reported PNIPAAm IPNs, the crosslinking design did not qualify them as DNs [96]. Furthermore, while these PNIPAAm IPNs achieved enhanced mechanical properties, equilibrium swelling was correspondingly decreased.

**Table 2.1.** Hydrogel composition

| | 1st Network | | 2nd Network | |
|---|---|---|---|---|
| Notation | %BIS | NP (size) | %BIS | NP (size) |
| SN | 4% | -- | -- | -- |
| DN | 4% | -- | 0.2% | -- |
| 50-1 | 4% | ~50 nm | 0.2% | -- |
| 50-2 | 4% | -- | 0.2% | ~50 nm |
| 200-1 | 4% | ~200 nm | 0.2% | -- |
| 200-2 | 4% | | 0.2% | ~200 nm |

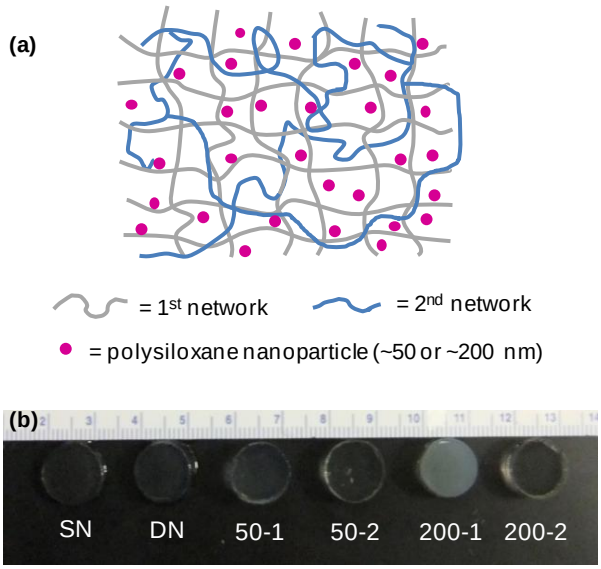


**Figure 2.1.** (a) Schematic depiction of double network (DN) hydrogels in which polysiloxane nanoparticles were introduced during formation of the "1st network" (i.e. *50-1* & *200-1*) or the subsequent "2nd network" (i.e. *50-2* & *200-2*). (b) Photograph of hydrogels series.

Herein, we report thermoresponsive PNIPAAm DN hydrogels containing inorganic polysiloxane nanoparticles (**Table 2.1, Figure 2.1a**). Colloidal polysiloxane nanoparticles with average diameters of ~50 nm[89] and ~200 nm [38] prepared *via* emulsion polymerization were utilized. Nanocomposite DN hydrogels were prepared with a tightly crosslinked PNIPAAm 1st network and a loosely crosslinked PNIPAAm 2nd network by altering the amount of BIS crosslinker. Nanoparticles were introduced during the formation of the 1st or 2nd network. The VPTT, morphology, equilibrium swelling, deswelling/reswelling kinetics, and mechanical properties were evaluated.

## 2.3. Materials and Methods

### *2.3.1. Materials*

Octamethylcyclotetrasiloxane ($D_4$) and 1,3,5,7-tetra-methyl-1,3,5,7 tetravinylcyclotetrasiloxane ($D_4^{vi}$) were purchased from Gelest, Inc. Brij 35, Brij 78, *N*-isopropylacrylamide (NIPAAm, 97%) and Tergitol NP-40 (70% in $H_2O$) were obtained from Aldrich. Dodecylbenzenesulfonic acid (DBSA, BIO-SOFT® S-101) was purchased from Stepan Co. Potassium persulfate ($K_2S_2O_8$) was purchased from Mallinchrodt Chemicals. *N,N'*-methylenebisacrylamide (BIS, 99%) was purchased from ACROS. 1-[4-(2-Hydroxy)-phenyl]-2-hydroxy-2-methyl-1-pro-pane-1-one (Irgacure 2959) was purchased from Ciba.

### *2.3.2. Synthesis of crosslinked polysiloxane colloidal nanoparticles*

Crosslinked polysiloxane nanoparticles having two different average diameters (~54 nm [89] and ~219 nm [38]) were prepared as previously reported.

### *2.3.3. Preparation of single network (SN) hydrogels*

SN hydrogels were prepared via *in situ* photocure of aqueous precursor solutions containing NIPAAm monomer, BIS crosslinker, Irgacure-2959 photoinitiator, DI water and optionally crosslinked polysiloxane nanoparticles (2 wt% solid nanoparticles based on NIPAAm weight). In a 50-mL round bottom (rb) flask equipped with a Teflon-covered stir bar, NIPAAm (1.0 g), BIS (0.04 g), and Irgacure-2959 (0.08 g) were

dissolved in DI water (the total volume equal to 7 mL including the volume of water introduced by the nanoparticle emulsion). Finally, the required amount of nanoparticle emulsion was optionally added.

Hydrogel sheets were prepared by pipetting the precursor solution into a rectangular mold formed by sandwiching polycarbonate spacers (1.5 mm thick) between two clamped glass microscope slides. The mold was submerged in an ice water bath (~7 $^{o}$C) and subjected to UV light (UV-Transilluminator, 6 mw/cm$^2$, 365 nm) for 30 min. After removal from the mold, the hydrogel sheet was rinsed with DI water and then soaked in DI water for 2 days with daily water changes to remove impurities.

For tensile tests, hydrogels were prepared with a "ring" geometry. First, hydrogels were prepared as a hollow tube with a double walled tubular mold composed of an inner glass mandrel (diameter = 3.2 mm) and an outer glass cylinder (diameter = 7.9 mm) secured with machined Teflon stoppers at each end. By removing one stopper, the tubular mold was filled with the precursor solution, stoppered, and photocured while submerged in an ice water bath (~7 °C) for 30 min under constant rotation such that each surface point received equal UV intensity and exposure time. The hydrogel tube was removed from the mold and similarly purified as above. For tensile tests of *SN*, ~ 3 mm wide pieces were cut from the central portion of the resulting hydrogel tube.

*2.3.4. Preparation of double network (DN) hydrogels*

The designated SN hydrogel was soaked in a solution of NIPAAm (6.0 g), BIS (0.012 g), Irgacure-2959 (0.24 g), DI water (the total volume equal to 21 mL including

the volume of water introduced by the nanoparticle emulsion) and optionally crosslinked polysiloxane nanoparticles (2 wt% solid nanoparticles based on NIPAAm weight) for 24 hr. The hydrogel sheet was then transferred to a rectangular mold (2.3 mm thick), photocured and purified as above.

For tensile tests, DN hydrogels with a ring geometry were prepared by soaking the previously prepared SN hydrogel tube in the aforementioned solution as above. The hydrogel tube was then transferred to a double walled tubular mold composed of an inner glass mandrel (diameter = 3.2 mm) and an outer glass cylinder (diameter = 12.5 mm), secured with Teflon stoppers at each end and cured as above (~7 °C, 30 min). Following purification, the central portion of the hydrogel tube was cut into ~ 3 mm wide pieces to produce the ring specimens.

*2.3.5. Extent of crosslinking*

The amount of uncrosslinked material in select hydrogels was determined by weight loss following soaking in dichloromethane ($CH_2Cl_2$). For a given hydrogel, three hydrogel discs (13 mm diameter, 1.5 mm thickness) were punched from a single hydrogel sheet with a die and dried in a vacuum oven [30 in. Hg, room temperature (RT), 24 hr] and weighed. Each dried discs was soaked in 10 mL of $CH_2Cl_2$ for 24 hr and weighed after similarly drying in a vacuum oven. The percentage of uncrosslinked material was calculated as the average weight difference of the extracted versus unextracted weight divided by the unextracted weight.

*2.3.6. Volume phase transition temperature (VPTT)*

The VPTT of swollen hydrogels was determined by differential scanning calorimetry (DSC, TA Instruments Q100). Water-swollen hydrogels were blotted with Kim Wipe and a small piece sealed in a hermetic pan. After cooling to -50 °C, the temperature was increased to 50 °C at a rate of 3 °C /min for 2 cycles. The resulting endothermic phase transition peak is characterized by the initial temperature at which the endotherm starts ($T_o$) and the peak temperature of the endotherm ($T_{max}$). Reported data is from the 2nd cycle.

*2.3.7. Morphology*

To retain their morphology, swollen hydrogel specimens were immersed in liquid nitrogen and subsequently freeze-dried with a lyophilizer (Labconco Centri Vap Gel Dryer System) overnight. Specimen cross-sections were subjected to Pt-sputter coating and viewed with a field emission scanning electron microscope (FEI Quanta 600 FE-SEM) at 10 keV accelerating voltage.

*2.3.8. Equilibrium swelling*

Three discs (13 mm diameter) were punched from a single sheet with a die. Each disc was placed in a sealed vial containing 20 mL DI water, immersed in a temperature controlled water bath for 24 hr at the designated temperature (10-50 °C), removed, blotted with a Kim Wipe to remove surface water and weighed ($W_t$). After the last

measurement, each disc was vacuum dried (30 in. Hg, 60 °C, 24 hr) and weighed ($W_d$). Equilibrium swelling ratio ($SR$) is defined as: $SR = W_t/W_d$.

*2.3.9. Kinetic deswelling*

Three discs (13 mm diameter) were prepared as above. Each disc was placed in a sealed vial containing 20 mL DI water, immersed in a water bath for 24 h at 22 °C to reach equilibrium ($W_s$) and quickly transferred into a 50 °C water bath. At 10, 20, 40, 80, 120, 180 min, each disc was removed, blotted with a Kim Wipe, immediately weighed ($W_t$) and returned to the vial for subsequent measurements. After 180 min, the discs were dried in a vacuum oven (30 in. Hg, 60 °C, 24 hr) and weighed ($W_d$). Water retention ($WR$) is defined as: $WR = (W_t - W_d)/W_s$.

*2.3.10. Kinetic re-swelling*

Three discs (13 mm diameter) were prepared as above. Each disc was placed in an open vial, dried in a vacuum oven (30 in. Hg, 60 °C, 24 hr) and weighed ($W_d$). To each vial was added 20 mL DI water and the sealed vial immersed in a water bath at 22 °C. At 10, 20, 40, 80, 120, 200, 320, 450 and 640 min, each disc was removed, blotted with a Kim Wipe and weighed ($W_t$). Kinetic reswelling ratio is defined as: $SR = W_t/W_d$.

*2.3.11. Dynamic mechanic analysis (DMA)*

Five discs (13 mm diameter) were prepared as above. DMA of discs was measured in the compression mode with a dynamic mechanical analyzer (TA

Instruments Q800) equipped with parallel-plate compression clamp with a diameter of 40 mm (bottom) and 15 mm (top). The swollen disc (13 mm diameter) was blotted with a Kim Wipe, clamped between the parallel plates and silicone oil placed around the exposed hydrogel edge to prevent dehydration. Following equilibration below the VPTT at 25 $^{\circ}$C (5 min), the specimens were tested in a multi-frequency-strain mode (1 to 25 Hz).

*2.3.12. Compression tests*

Three discs (13 mm diameter) were prepared as above. Compressive tests were performed with an Instron 3340 at RT. A swollen disc (13 mm diameter) was blotted with a Kim Wipe and clamped between the parallel plates with an initial pre-load force of ~0.5 N. Compressive strain was applied at a rate of 1 mm/min until the disc fractured. The following parameters were determined: (1) compressive modulus; (2) ultimate compressive strength (UCS), and (3) % strain at break. The modulus was obtained from the slope of the stress-strain curve between 0 and 10% strain [94].

*2.3.13. Tensile tests*

A ring geometry rather than a rectangular strip or dog bone was used to measure tensile properties for improved accuracy [38, 97]. Three hydrogel rings (~3 mm width) were cut from the central portion of the designated hydrogel tube using a razor blade and dimensions measured with an electronic caliper. The ring was blotted with a Kim Wipe and loaded onto custom aluminium bars gripped directly into DMA tension clamps so

that the upper and lower bars were located inside the ring. At RT, samples were subjected to a constant strain (1 mm/min) until they broke at the center of one side of the ring. Stress was calculated from the measured force divided by the cross-sectional area of two rectangles with sides equal to the width and wall thickness of the ring. The gauge length corresponded to the outer diameter of the ring less the wall thickness. The following parameters were determined: (1) tensile modulus, (2) ultimate tensile strength (*UTS*), and (3) % strain at break. The tensile modulus was obtained from the slope of the linear part of the stress-strain curve between 0 and 10% strain. The *UTS* represents the maximum stress prior to failure. % Strain at break was calculated from the measured displacement divided by the gauge length.

**Table 2.2.** VPTT and mechanical properties of hydrogels

| | **VPTT** | | **Compressive Properties** | | | **Tensile Properties** | | |
|---|---|---|---|---|---|---|---|---|
| Hydrogel | $T_o$ (°C) | $T_{max}$ (°C) | Modulus (kPa) | UCS (kPa) | %strain @ break | Modulus (kPa) | UTS (kPa) | %strain @ break |
| **SN** | 32.0 | 33.9 | 81 ± 14 | 144 ± 12 | 57 ± 1 | 19.7 ± 2.0 | 6.4 ± 0.5 | 26 ± 3 |
| **DN** | 32.4 | 34.0 | 188 ± 7 | 452 ± 56 | 52 ± 3 | 26.6 ± 0.5 | 8.6 ± 1.4 | 32 ± 4 |
| **50-1** | 32.5 | 33.6 | 162 ± 11 | 473 ± 59 | 57 ± 2 | 21.7 ± 1.6 | 7.6 ± 1.6 | 36 ± 3 |
| **50-2** | 32.1 | 33.5 | 175 ± 16 | 474 ± 60 | 52 ± 1 | 25.9 ± 1.0 | 7.9 ± 0.5 | 31 ± 4 |
| **200-1** | 32.3 | 33.6 | 181 ± 7 | 443 ± 48 | 51 ± 3 | 21.0 ± 1.5 | 7.5 ± 2.7 | 35 ± 9 |
| **200-2** | 32.2 | 33.6 | 165 ± 7 | 600 ± 7 | 54 ± 2 | 22.7 ± 1.1 | 9.9 ± 1.3 | 40 ± 1 |

**Table 2.3.** Gel content of SN and DN hydrogel series.

| | 1st Network | | 2nd Network | | Uncrosslinked Content |
|---|---|---|---|---|---|
| Notation | %BIS | NP (size) | %BIS | NP (size) | % |
| **SN** | 4% | -- | -- | -- | 5.8±0.3 |
| **DN** | 4% | -- | 0.2% | -- | 0.4±0.2 |
| **50-1** | 4% | ~50 nm | 0.2% | -- | 1.6±1.2 |
| **50-2** | 4% | -- | 0.2% | ~50 nm | 1.2±0.8 |
| **200-1** | 4% | ~200 nm | 0.2% | -- | 1.5±0.8 |
| **200-2** | 4% | -- | 0.2% | ~200 nm | 0.6±0.2 |

## 2.4. Results and Discussion

### *2.4.1. Preparation of SN and DN hydrogels*

SN hydrogels (including "*SN*") were formed by photo-polymerization of aqueous solutions containing NIPAAm monomer and BIS crosslinker (4 wt% based on NIPAAm) and optionally polysiloxane nanoparticles (**Table 2.1**, **Figure 2.1**). DN hydrogels (including "*DN*") were formed sequentially in two steps by swelling the

designated SN hydrogel with an aqueous solution containing NIPAAm and BIS crosslinker (0.2 wt% based on NIPAAm) and optionally polysiloxane nanoparticles followed by subsequent photocure. For all DN hydrogels, the % uncrosslinked material extracted was less than 2% (**Table 2.3**). The DN hydrogels are comprised of a relatively high crosslink density 1st network and an interpenetrating low crosslink density 2nd network (**Figure 2.1a**). The SN and DN hydrogels prepared without nanoparticles were optically clear indicative of a homogeneous morphology associated with curing at low temperatures ($T_{prep}$ < 20 °C) (**Figure 2.1b**) [38, 98, 99]. Upon incorporation of polysiloxane nanoparticles, the *DN* hydrogels became somewhat opaque and, as expected, more so with the larger ~200 nm nanoparticles. It was observed that DN hydrogels in which the polysiloxane nanoparticles were introduced into the 1st network (i.e. *50-1* and *200-1*) were relatively more opaque versus the corresponding DN hydrogel in which the nanoparticles were incorporated into the 2nd network (i.e. *50-2* and *200-2*, respectively). Because of the relatively high crosslink density of the 1st network, subsequent integration of polysiloxane nanoparticles was apparently somewhat inhibited. However, *50-2* and *200-2* were more opaque versus *DN* (no nanoparticles), indicating incorporation of some polysiloxane nanoparticles.

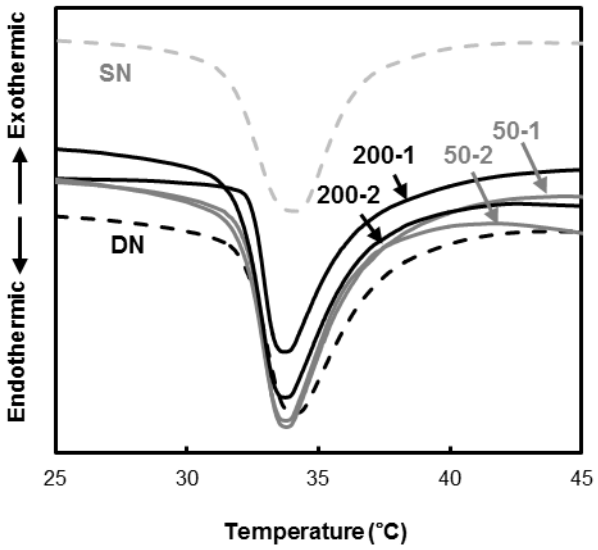


**Figure 2.2.** DSC thermograms of hydrogels.

*2.4.2. VPTT*

When heated above its VPTT, PNIPAAm hydrogels exhibit an endothermic peak due to breaking of the hydrogen bonds of surrounding water molecules [100, 101]. Measured by DSC, the onset ($T_o$) or the maximum temperature ($T_{max}$) of the endothermic peak designates the VPTT [102-104]. In this way, the VPTT of swollen hydrogels were determined (**Table 2.2., Figure 2.2**). When the hydrogel matrix was changed from a SN ("*SN*") to DN ("*DN*") design, the VPTT was not altered. The VPTT was also unchanged when polysiloxane nanoparticles were incorporated into DN hydrogels. This effect was similarly observed when ~50 and 200 nm polysiloxane nanoparticles were incorporated into SN hydrogels [38, 89]. The lack of change to the VPTT is attributed to the discrete

nature of the nanoparticles which apparently do not interfere with dissociation of water molecules around the PNIPAAm propyl moieties during heating.

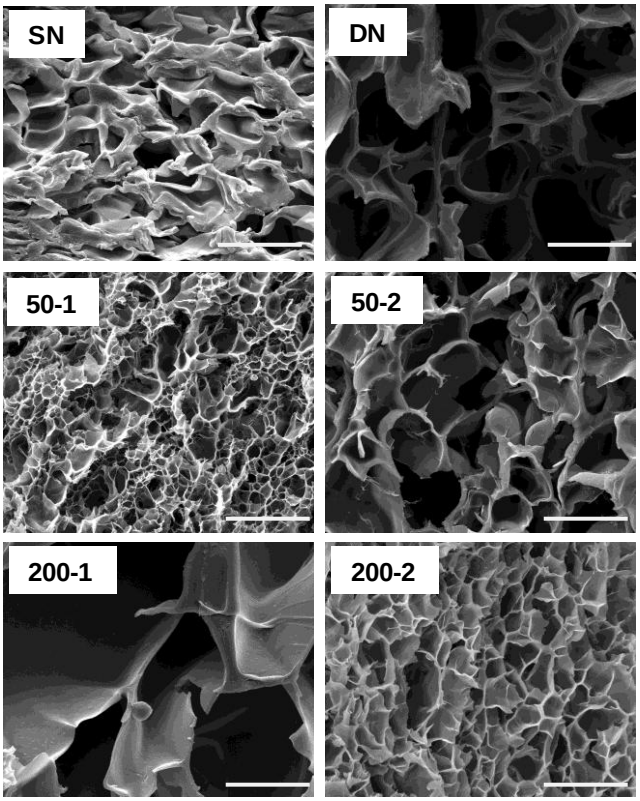


**Figure 2.3.** SEM micrographs of hydrogels. All scale bars = 20 μm.

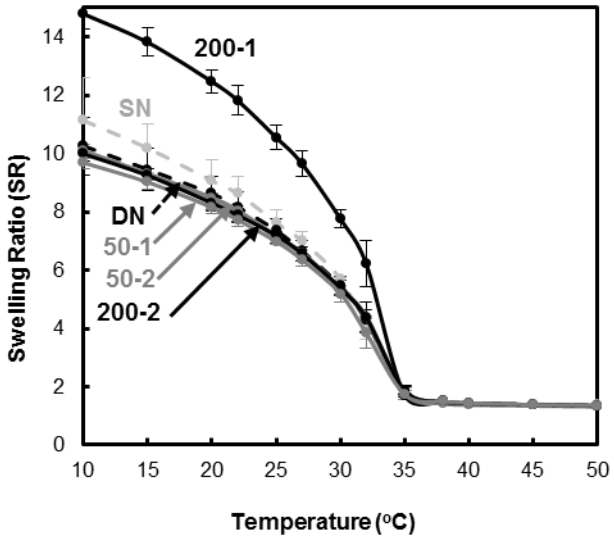


**Figure 2.4.** Hydrogel equilibrium swelling ratio (by mass).

*2.4.3. Morphology*

The morphology of hydrogels was studied by SEM. Morphology was dramatically changed according to composition (**Figure 2.3**). For *200-1*, pores were

notably larger versus other hydrogels. This may be the result of its combination of larger nanoparticles (i.e. ~200 nm) and higher nanoparticle content (versus *200-2*) which facilitated the expansion of the pores due to the hydrophobicity of the polysiloxane nanoparticles.

### *2.4.4. Equilibrium swelling*

Equilibrium swelling ratios of the hydrogels was measured gravimetrically from 10 to 50 $^{o}$C (**Figure 2.4**). At temperatures below the VPTT (~33 ºC), the hydrogels exist in a swollen state. Enhanced swelling below the VPTT is desirable for PNIPAAm-based hydrogels in applications involving transport and delivery. *DN* did not exhibit enhanced swelling versus *SN*. Thus, the enhanced swelling of previously reported DN hydrogel systems likely stems from the electrostatic nature of the ionizable network [91-93]. However, for *200-1*, the swelling ratio was dramatically enhanced below the VPTT and without compromising the extent of deswelling above the VPTT. The enhanced swelling of *200-1* may be explained by its particularly large pores (**Figure 2.3**).

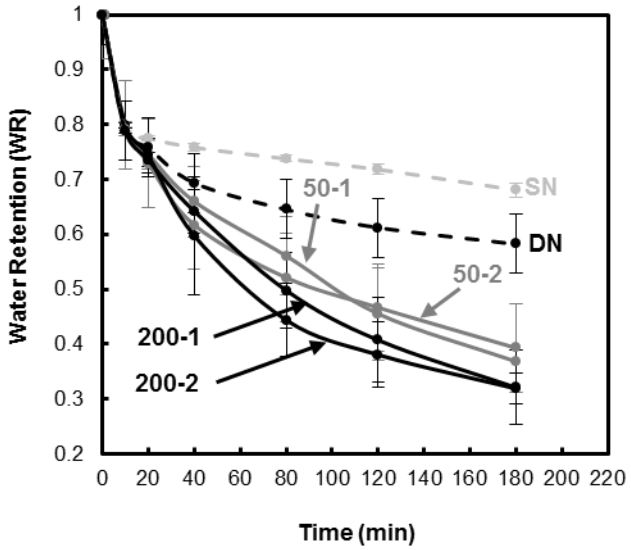


**Figure 2.5.** Hydrogel deswelling kinetics at 50 °C (by mass).

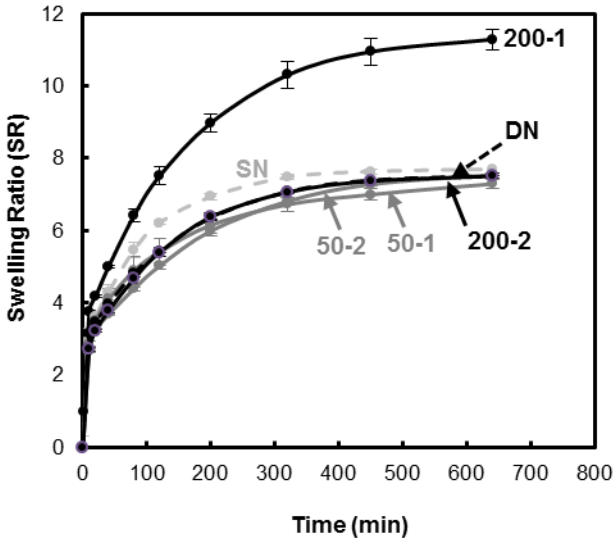


**Figure 2.6.** Hydrogel reswelling kinetics at 22 °C (by mass).

*2.4.5. Kinetic deswelling-re-swelling properties*

A rapid and extensive response to thermal modulation (i.e. thermosensitivity) of PNIPAAm-based hydrogels is essential for release and delivery applications. The thermosensitivity of hydrogels were determined by measuring the rate and extent to which they deswelled at 50 ºC (> VPTT) (**Figure 2.5**) and subsequently reswelled at 22 ºC (< VPTT) (**Figure 2.6**).

*DN* exhibited an enhanced rate and extent of deswelling versus *SN* due to the former's crosslink inhomogeneity. Furthermore, upon incorporation of polysiloxane nanoparticles, the resulting DN hydrogels exhibited an additional increase deswelling. The hydrophobicity of the nanoparticles may facilitate water expulsion during deswelling. DN hydrogels containing ~200 nm nanoparticles exhibited somewhat enhanced deswelling versus the corresponding DN hydrogels containing ~50 nm nanoparticles.

As with equilibrium swelling, the rate and extent of reswelling of *DN* not enhanced versus that of *SN*. In most cases, incorporation of polysiloxane nanoparticles into DN hydrogels did not significantly change reswelling behavior. However, *200-1* exhibited a pronounced increase in the rate as well as extent of swelling. The enhanced thermosensitivity of *200-1* is attributed to its particularly large pores (**Figure 2.3**).

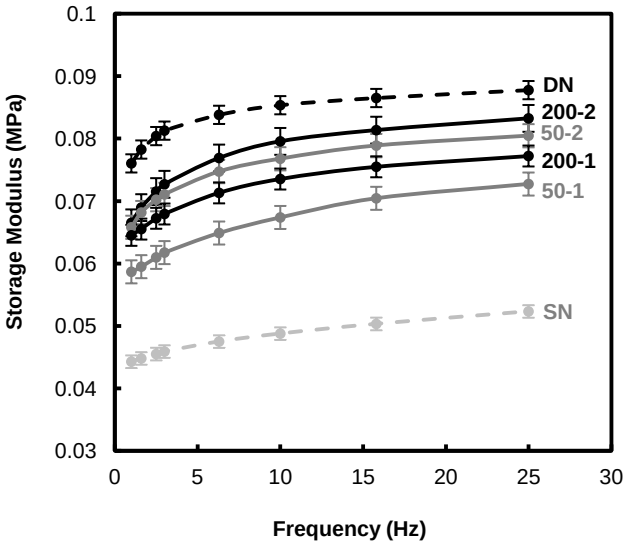


**Figure 2.7.** Storage modulus (G') of hydrogels in the compression mode.

*2.4.6. Mechanical properties*

Mechanical properties of PNIPAAm-based hydrogels are critical to maintain structural integrity when subjected to mechanical forces both *in vitro* and *in vivo*. During DMA, hydrogel stiffness was measured in terms of the storage modulus (*G'*) as a function of frequency of the applied strain in compression (**Figure 2.7**). G' of *DN* was nearly twice that of *SN*. Because the swelling ratio of *DN* and *SN* are very similar at RT, the enhanced stiffness of *DN* is attributed to its asymmetrically crosslinked network rather than reduced hydration [92, 105]. With the exception of *200-1*, incorporation of polysiloxane nanoparticles did not substantially change the RT swelling ratio of DN

hydrogels versus that of *DN* and *SN*. However, the *G'* of these DN hydrogels were lower than that of *DN* but remained higher than that of *SN*. It was also observed that for a given nanoparticle size, their incorporation into the 2nd rather than the 1st network produced DN hydrogels with higher *G'* values. As noted by their relative opacity, less nanoparticles are incorporated into the DN hydrogel when introduced during formation of the 2nd network. Apparently, nanoparticles somewhat alter the asymmetrically crosslinked network of the PNIPAAm matrix so as to diminish its ability to resist deformation.

As was observed for G', the compressive and tensile moduli of all DN hydrogels were greater than that of *SN* (**Table 2.2**). Quasi-static compression and tensile tests additionally permit assessment of strength. Ultimate compressive strength (UCS) has been observed to be dramatically enhanced for previously reported DN hydrogels.[91-93] This is attributed to the ability of the asymmetrically crosslinked networks to dissipate the applied force [92, 105]. *UCS* and *UTS* of all DN hydrogels were dramatically enhanced versus that of *SN*. *200-2* exhibited particularly high strength. However, given the substantially higher swelling of *200-1*, its high moduli and strength values are particularly notable.

## 2.5. Conclusions

Thermoresponsive nanocomposite double network (DN) PNIPAAm hydrogels were prepared by introducing polysiloxane nanoparticles (~50 nm and ~200 nm) during formation of the 1st, tightly crosslinked network or the 2nd, loosely crosslinked network.

Nanoparticles were more readily incorporated during formation of the 1st network. Neither the *DN* matrix nor nanoparticles altered the convenient VPTT of conventional, single network (SN) PNIPAAm hydrogels. However, other key physical properties were enhanced. In the absence of nanoparticles, a DN hydrogel (i.e. *DN*) essentially maintained equilibrium swelling and reswelling kinetics but exhibited an increase in the extent and rate of deswelling as well as an increase in hydrogel stiffness and strength. Incorporation of polysiloxane nanoparticles into DN hydrogels further altered these properties depending on size and whether introduced during formation of the 1st or 2nd network. The DN hydrogels formed with ~200 nm polysiloxane nanoparticles in the 1st network (i.e. *200-1*) exhibited exceptional properties. For *200-1*, equilibrium swelling was dramatically enhanced as well as deswelling/reswelling kinetics. Despite higher equilibrium swelling at RT, measured modulus and strength values surpassed that of the SN hydrogel (i.e. *SN*).

CHAPTER III

# ULTRA-STRONG THERMORESPONSIVE DOUBLE NETWORK HYDROGELS*

## 3.1. Overview

Thermoresponsive poly(*N*-isopropylacrylamide) (PNIPAAm) hydrogels are widely studied smart materials, particularly for biomedical applications, but are limited by their mechanical strength. In this study, double network (DN) hydrogels were prepared with an asymmetric crosslink design and inclusion of an electrostatic co-monomer, 2-acrylamido-2-methylpropane sulfonic acid (AMPS). These P(NIPAAm-*co*-AMPS)/PNIPAAm DN hydrogels were sequentially formed with a tightly crosslinked 1st network comprised of variable levels of AMPS (100:0 to 25:75 wt% ratio of NIPAAm:AMPS) and a loosely crosslinked 2nd network comprised of PNIPAAm. The impact of AMPS content in the 1st network on the volume phase transition temperature (VPTT), morphology, deswelling-reswelling kinetics and mechanical properties was evaluated. Without substantially altering the VPTT of conventional PNIPAAm hydrogels but with improving thermosensitivity, the DN hydrogel formed with 25:75 wt% of NIPAAm:AMPS achieved exceptional strength, high modulus and high % strain at break.

* Reprinted with permission from "Ultra-strong thermoresponsive double network hydrogels" by Fei R, George JT, Park J, Means AK, Grunlan MA, 2013. *Soft Matter*, 9, 2912-9, Copyright 2014 by the Royal Society of Chemistry.

### 3.2. Introduction

In response to temperature change, thermoresponsive hydrogels reversibly switch from a water-swollen, hydrophilic state to a deswollen, hydrophobic state [39, 42]. Thermoresponsive hydrogels are prepared by crosslinking polymers that exhibit a lower critical solubility temperature (LCST) such as poly(*N*-isopropyl-acrylamide (PNIPAAm; LCST, ~ 32 °C) [106]. Thermal modulation of PNIPAAm hydrogels above and below its volume phase transition temperature (VPTT, ~33-35 °C) causes its reversible dewelling and reswelling, respectively [44, 45]. Because of its convenient VPTT, PNIPAAm hydrogels are particularly useful as smart materials for various biological applications [46], including: microfluidic actuation [48-50], separation [51, 52], controlled drug delivery [53-55], cell sheet tissue engineering [29, 56], anti-fouling coatings [58, 59, 107] and "self-cleaning" membranes for implanted biosensors [60-63].

Unfortunately, conventional PNIPAAm hydrogels prepared via copolymerization of *N*-isopropylacrylamide (NIPAAm) and a crosslinker such as *N*,*N*'-methylenebisacrylamide (BIS) exhibit relatively poor mechanical properties in the swollen state [108, 109]. Improving the mechanical strength as well as stiffness (i.e. modulus) of PNIPAAm hydrogels would enhance their utility. However, this must not be achieved to the detriment of thermosensitivity (i.e. rate and extent of deswelling and reswelling) which is already limited for crosslinked PNIPAAm hydrogels [70, 108]. This presents a significant challenge. For instance, the mechanical properties of PNIPAAm hydrogels are often compromised by strategies used to enhance the thermosensitivity (without altering the VPTT), including: comb-type networks [68, 69, 110],

heterogeneous morphologies [72, 73, 111, 112], poration [74-76] or open channel structures [78].

Interpenetrating polymer networks (IPNs) are comprised of two crosslinked networks held together by inter-network entanglements [113]. Although PNIPAAm IPNs exhibited enhanced mechanical properties, their swelling was decreased [96]. Compared to conventional single network (SN) hydrogels or even IPN hydrogels, double network (DN) hydrogels display enhanced mechanical properties as well as a high degree of swelling [34, 35, 114]. A class of IPNs, DN hydrogels are comprised of a neutral and a polyelectrolyte network with one network more highly crosslinked than the other. Several DN hydrogel systems have been reported but none are thermoresponsive. The most extensively studied DN hydrogel system is that reported by Gong and co-workers consisting of a tightly crosslinked, ionizable 1$^{st}$ network comprised of poly(2-acrylamido-2-methylpropane sulfonic acid) (PAMPS) and a sparsely crosslinked, neutral 2$^{nd}$ network comprised of poly(acrylamide) (PAAm) (i.e. PAMPS/PAAm) [92]. Other DN hydrogels include PAMPS/poly(*N,N'*-dimethylacrylamide) (PDMAAm) [94] and modified hyaluronan (HA)/PDMAAm [95]. Frank and co-workers have reported DN hydrogels based on neutral poly(ethylene oxide) (PEO) as the tightly crosslinked 1$^{st}$ network and ionizable poly(acrylic acid) (PAA) as the loosely crosslinked 2$^{nd}$ network (i.e. PEO/PAA DN) [93]. Recently, Frank and co-workers reported a pH- and temperature "dual responsive" PNIPAAm/PAA hydrogel system which is an IPN due to the constant level of crosslinking in the 1$^{st}$ and 2$^{nd}$ networks [115].

Of late, we have reported the first thermoresponsive PNIPAAm DN hydrogels [116]. These were comprised of a tightly crosslinked PNIPAAm 1st network and a loosely crosslinked PNIPAAm 2nd network. Optionally, colloidal polysiloxane nanoparticles (~50 and 200 nm diameters) were incorporated during formation of the 1st or 2nd network to form nanocomposite DN hydrogels. Compared to the conventional PNIPAAm SN hydrogel, the PNIPAAm DN hydrogel exhibited similar swelling but improved strength and modulus. Inclusion of nanoparticles improved thermosensitivity without altering the VPTT but did not significantly improve mechanical properties relative to the DN hydrogel.

In this work, we report the formation of P(NIPAAm-*co*-AMPS)/PNIPAAm DNs to achieve improved mechanical properties versus PNIPAAm SN or DN hydrogels but with a concomitant improvement in thermosensitivity. These *DNs* are comprised of tightly crosslinked, ionized 1st network [P(NIPAAm-*co*-AMPS)] and a loosely crosslinked, interpenetrating 2nd network [PNIPAAm]. While P(NIPAAm-*co*-AMPS) SN hydrogels have been previously reported their mechanical properties were not investigated [117]. AMPS is a strong electrolyte whose sulfonate groups completely dissociate over a wide pH range [118, 119]. In aqueous solution, polymers based on AMPS exhibit a marked coil expansion in aqueous solutions and networks are expanded [120]. This behavior is attributed to the strong electrostatic repulsive forces which give rise to an increase in osmotic pressure [118]. As a result, AMPS-containing SN hydrogels such as P(AAm-*co*-AMPS) exhibit enhanced swelling with increased AMPS content [118-121]. In addition, P(AAm-*co*-AMPS) DN hydrogels exhibit notably high

strength as well as modulus values [90, 92, 122, 123]. Thus, in this work, AMPS was utilized to impart these properties to this PNIPAAm-based DN system.

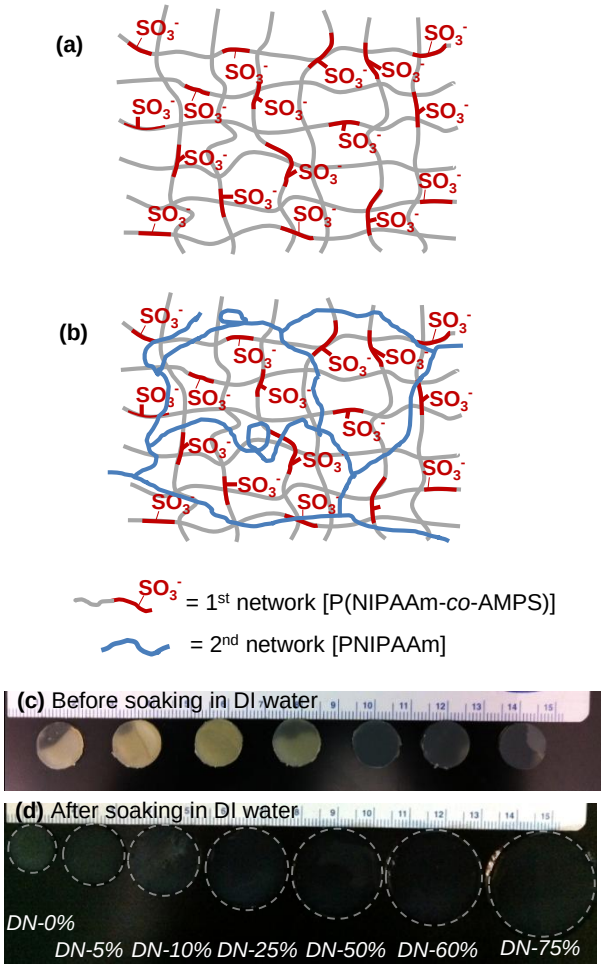


**Figure 3.1.** Schematic depiction of P(NIPAAm-*co*-AMPS)/PNIPAAm double network (DN) hydrogels. Sequential formation of (a) 1st network (i.e. formation of single network, SN) and (b) subsequent formation of 2nd network (i.e. formation of DN). Photograph of DN hydrogels: (c) discs punched from a sheet immediately following crosslinking of 2nd network and (d) after subsequently soaking in DI water for 48 hr. Per Table 3.1, DN hydrogels are denoted as "DN-X%" where X% equals the wt% of AMPS in the 1st network.

**Table 3.1.** Composition, *VPTT* and mechanical of SN and DN

| Notation | 1st Network[a] | | 2nd Network[b] | ***VPTT*** | | **Compressive Properties** | | |
|---|---|---|---|---|---|---|---|---|
| | **wt% ratio** NIPAAm:AMPS | **mol%** ratio NIPAAm:AMPS | **wt% ratio** NIPAAm:AMPS | $T_o$ (°C) | $T_{max}$ (°C) | *Modulus* (MPa) | *UCS* (MPa) | *%strain at break* |
| ***SN-0%*** | 100:0 | 100:0 | 100:0 | 32.0 | 33.9 | 0.081 ± 0.014 | 0.144 ± 0.012 | 57 ± 1 |
| ***DN-0%*** | 100:0 | 100:0 | 100:0 | 32.4 | 34.0 | 0.188 ± 0.007 | 0.452 ± 0.056 | 52 ± 3 |
| ***DN-5%*** | 95:5 | 97:3 | 100:0 | 31.6 | 33.4 | 0.192 ± 0.024 | 0.259 ± 0.029 | 40 ± 2 |
| ***DN-10%*** | 90:10 | 94:6 | 100:0 | 31.5 | 33.1 | 0.277 ± 0.060 | 0.563 ± 0.026 | 52 ± 7 |
| ***DN-25%*** | 75:25 | 85:15 | 100:0 | 30.9 | 32.8 | 0.341 ± 0.048 | 0.784 ± 0.004 | 46 ± 1 |
| ***DN-50%*** | 50:50 | 65:35 | 100:0 | 31.5 | 33.0 | 0.311 ± 0.035 | 2.532 ± 0.314 | 73 ± 5 |
| ***DN-60%*** | 40:60 | 55:45 | 100:0 | 31.5 | 33.0 | 0.303 ± 0.005 | 3.128 ± 0.545 | 71 ± 5 |
| ***DN-75%*** | 25:75 | 38:62 | 100:0 | 31.6 | 32.9 | 0.085 ± 0.018 | 17.50 ± 2.986 | 95 ± 2 |

[a]wt%BIS: = 4%. [b]wt% BIS: 0.2%

Herein, P(NIPAAm-*co*-AMPS)/PNIPAAm DN networks were formed with a tightly crosslinked 1st network comprised of variable levels of AMPS (100:0 to 25:75 wt% ratio of NIPAAm:AMPS) and a loosely crosslinked 2nd network comprised of PNIPAAm. The VPTT, morphology, equilibrium swelling, deswelling-reswelling kinetics and mechanical properties were evaluated.

## 3.3. Materials and Methods

### *3.3.1. Materials*

*N*-isopropylacrylamide (NIPAAm, 97%) was obtained from Aldrich. Acrylamido-2-methylpropane sulfonic acid (AMPS, 97%) and *N,N'*-methylenebisacrylamide (BIS, 99%) were purchased from ACROS. 1-[4-(2-

Hydroxyethoxy)-phenyl]-2-hydroxy-2-methyl-1-pro-pane-1-one (Irgacure 2959) was purchased from BASF.

### *3.3.2. Preparation of single network (SN) hydrogels*

SN hydrogels (including those that serve as the 1st network of DN hydrogels) were prepared *via in situ* photocure of aqueous precursor solutions containing NIPAAm monomer, AMPS monomer (optional), BIS crosslinker, Irgacure-2959 photo-initiator and DI water (**Figure 3.1a**). In a 50-mL round bottom (rb) flask equipped with a Teflon-covered stir bar, NIPAAm/AMPS (total weight equal to 1.0 g), BIS (0.04 g), and Irgacure (0.08 g) were dissolved in DI water (7.0 mL). The wt% ratio of NIPAAm to AMPS was systematically varied (**Table 3.1**).

Hydrogel sheets were prepared by pipetting the precursor solution into a rectangular mold formed by sandwiching polycarbonate spacers (1.5 mm thick) between two clamped glass microscope slides. The mold was submerged in an ice water bath (~7 $^{o}$C) and subjected to UV light (UV-Transilluminator, 6 mw/cm2, 365 nm) for 30 min. After removal from the mold, the hydrogel sheet was rinsed with DI water and then soaked in DI water for 2 days with daily water changes to remove impurities. Specimens used for analyses were taken from hydrogel sheets following soaking.

### *3.3.3. Preparation of double network (DN) hydrogels*

The designated SN hydrogel (i.e. the 1$^{st}$ network) was soaked in a solution of NIPAAm (6.0 g), BIS (0.012 g), Irgacure-2959 (0.24 g), DI water (21 mL) for 24 hr. The

hydrogel sheet was then transferred to a rectangular mold (2.3 mm thick), photocured and purified as above (**Figure 3.1b**). Specimens used for analyses were taken from hydrogel sheets following soaking.

### *3.3.4. Extent of crosslinking*

The percentage of uncrosslinked material (i.e. % extractables) in select hydrogels was determined by weight loss following soaking in dichloromethane ($CH_2Cl_2$). For a given hydrogel, three hydrogel discs (13 mm diameter, 1.5 mm thickness) were punched from a single hydrogel sheet with a die and dried in a vacuum oven [30 in. Hg, room temperature (RT), 24 hr] and weighed. Each dried disc was soaked in 10 mL of $CH_2Cl_2$ for 24 hr and weighed after similarly drying in a vacuum oven. The % extractables was calculated as the average weight difference of the extracted versus unextracted weight divided by the unextracted weight.

### *3.3.5. Volume phase transition temperature (VPTT)*

The VPTT of swollen hydrogels was determined by differential scanning calorimetry (DSC, TA Instruments Q100). Water-swollen hydrogels were blotted with a Kim Wipe and a small piece sealed in a hermetic pan. After cooling to -50 $^{o}$C, the temperature was increased to 50 $^{o}$C at a rate of 3 $^{o}$C /min for 2 cycles. The resulting endothermic phase transition peak was characterized by the initial temperature at which the endotherm starts ($T_o$) and the peak temperature of the endotherm ($T_{max}$). Reported data are from the 2$^{nd}$ cycle.

*3.3.6. Morphology*

Hydrogel discs (13 mm diameter) were punched from a hydrogel sheet. Discs were submerged in liquid nitrogen for 1 min and immediately freeze-dried (Labconco Freezone 2.5) overnight. Cross-sections were prepared by cutting with a clean razor blade. Specimen cross-sections were subjected to Pt-sputter coating and viewed with a field emission scanning electron microscope (FEI Quanta 600 FE-SEM) at accelerated electron energy of 10 keV.

*3.3.7. Kinetic deswelling*

Three discs (13 mm diameter) were prepared as above. Each disc was placed in a sealed vial containing 20 mL DI water, immersed in a water bath for 24 hr at 22 $^{o}$C to reach equilibrium ($W_s$) and quickly transferred into a 50 $^{o}$C water bath. At 10, 20, 40, 80, 120 and 180 min, each disc was removed, blotted with a Kim Wipe, immediately weighed ($W_t$) and returned to the vial for subsequent measurements. After 180 min, the discs were dried in a vacuum oven (30 in. Hg, 60 $^{o}$C, 24 hr) and weighed ($W_d$). Water retention (WR) is defined as: $WR = (W_t - W_d)/W_s$.

*3.3.8. Kinetic reswelling*

Three discs (13 mm diameter) were prepared as above. Each disc was placed in an open vial, dried in a vacuum oven (30 in. Hg, 60 $^{o}$C, 24 hr) and weighed ($W_d$). To each vial was added 20 mL DI water and the sealed vial immersed in a water bath at 22

$^{o}$C. At 10, 20, 40, 80, 120, 200, 320, 450 and 640 min, each disc was removed, blotted with a Kim Wipe and weighed ($W_t$). Kinetic re-swelling ratio is defined as: SR = $W_t/W_d$.

*3.3.9. Dynamic mechanical analysis (DMA)*

Five discs (13 mm diameter) were prepared as above. DMA of the discs was performed in the compression mode with a dynamic mechanical analyzer (TA Instruments Q800) equipped with parallel-plate compression clamp with a diameter of 40 mm (bottom) and 15 mm (top). The swollen disc was blotted with a Kim Wipe, clamped between the parallel plates and silicone oil placed around the exposed hydrogel edge to prevent dehydration. Following equilibration below the VPTT at 25 $^{\circ}$C (5 min), the specimens were tested in a multi-frequency-strain mode (1 to 25 Hz).

*3.3.10. Compression tests*

Three discs (6 mm diameter) were punched from a single sheet with a die. Compressive tests were performed with an Instron 3340 at RT. A swollen disc (6 mm diameter) was blotted with a Kim Wipe and clamped between the parallel plates with an initial pre-load force of ~0.5 N. Compressive strain was applied at a rate of 1 mm/min until the disc fractured. The following parameters were determined: (1) compressive modulus (*E*); (2) ultimate compressive strength (*UCS*), and (3) % strain at break. The modulus was obtained from the slope of the stress-strain curve from 0-10% strain [94].

## 3.4. Results and Discussion

### *3.4.1. Preparation of SN and DN hydrogels*

Conventional PNIPAAm SN hydrogels (*SN-0%*) were formed by photopolymerization of aqueous solutions containing NIPAAm and BIS crosslinker (4 wt% based on NIPAAm weight) (**Table 3.1**). *SN-0%* served as a conventional PNIPAAm *SN* control for all analyses. In the case DN hydrogel fabrication, the 1st network (i.e. *SN*) was likewise formed but with the monomer being a combination of a varying ratio of NIPAAm:AMPS (100:0 to 25:75 wt%). Subsequent soaking of these 1st networks in the 2nd network solution comprised of NIPAAm and BIS crosslinker (0.2 wt% based on NIPAAm weight) yielded the corresponding DN hydrogels (**Table 3.1**, **Figure 3.1a & 3.1b**). Per **Table 3.1**, DN hydrogels are denoted as "*DN-X%*" where *X%* equals the wt% of AMPS in the 1st network. *DN-0%* served as a PNIPAAM *DN* control for all analyses. The remaining DN hydrogels are comprised of a highly crosslinked, P(NIPAAm-*co*-AMPS) 1st network of varying amounts of ionized sulfonate groups and an interpenetrating, loosely crosslinked, neutral PNIPAAM 2nd network.

For P(NIPAAm-*co*-AMPS)/PNIPAAm DN hydrogels, a 25:75 wt% ratio of NIPAAm:AMPS was selected as the maximum level of AMPS in the 1st network. This was based on our observation that 1st networks (i.e. SNs) prepared with higher levels of AMPS produced poorly cured hydrogels. We verified that the 1st network used to eventually form *DN-75%* (i.e. NIPAAm:AMPS = 25:75 wt%) contained low levels of uncrosslinked material (2% extractables) (**Table 3.2**). However, 1st networks prepared

with 15:85 and 5:95 wt% of NIPAAm:AMPS indeed produced higher % extractables (4 and 32%, respectively).

**Table 3.2.** Percent extractables of P(NIPAAm-*co*-AMPS) prepared with higher levels of AMPS.

| Notation | 1st Network[a] | | 2nd Network[b] | % Extractables |
|---|---|---|---|---|
| | **wt% ratio** NIPAAm:AMPS | *mol% ratio NIPAAm: AMPS* | **wt% ratio** NIPAAm:AMPS | |
| **DN-65%** | 35:65 | *50:50* | 100:0 | 2.0 ± 1.8 % |
| **DN-70%** | 30:70 | *44:56* | 100:0 | 0.3 ± 0.6% |
| **DN-75%** | 25:75 | *38:62* | 100:0 | 2.0 ± 2.4% |
| **DN-85%** | 15:85 | *24:76* | 100:0 | 3.9 ± 0.1% |
| **DN-95%** | 5:95 | *9:91* | 100:0 | 32.2 ± 16.7% |

All hydrogels were photocured at low temperatures ($T_{prep}$ < 20 °C) to obtain a homogeneous rather than a heterogeneous morphology [98, 99]. Immediately following cure, hydrogel discs were somewhat iridescent due to the presence of unreacted NIPAAm monomer (**Figure 3.1c**). However, following soaking in DI water to remove impurities, all hydrogels were rather transparent which is consistent with homogeneous hydrogels (**Figure 3.1d**). Notably, the extent to which the freshly cured hydrogel discs swelled (i.e. increased in diameter) after soaking in DI water dramatically increased with higher levels of AMPS. This is attributed to the greater expansion of the 1st network due to a rise in electrostatic repulsive forces with AMPS levels which produces an increase in osmotic pressure [124].

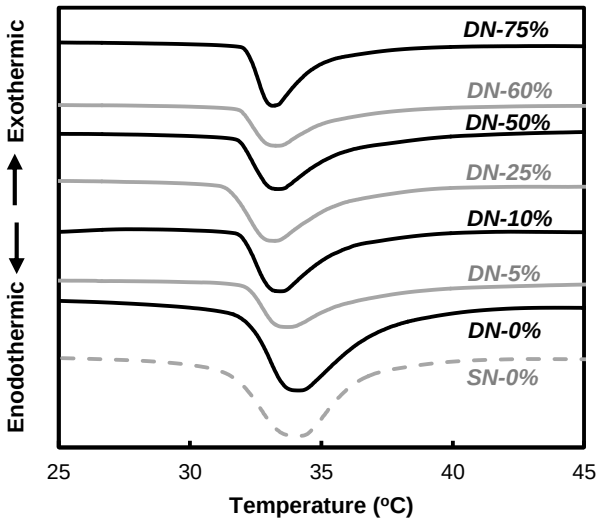


**Figure 3.2a.** DSC thermograms of hydrogels.

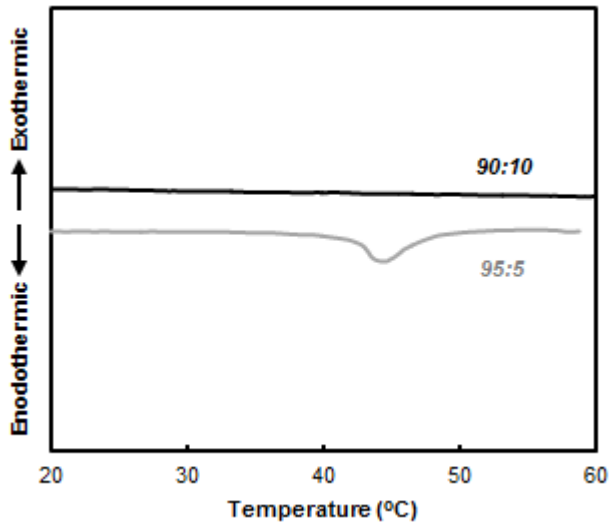


**Figure 3.2b.** Hydrogel deswelling kinetics at 50 °C (by mass). All scale bars = 50 μm.

*3.4.2. VPTT*

When heated above its VPTT, thermoresponsive PNIPAAm hydrogels deswell due to breaking of hydrogen bonds of surrounding water molecules and subsequent increase in hydrophobic interactions. As recorded by DSC, an endothermic peak accompanies this process and VPTT is defined in terms of the onset ($T_o$) and the maximum temperature ($T_{max}$) of the endothermic peak [105, 125]. As expected for "PNIPAAm-only" hydrogels (i.e. *SN-0%* and *DN-0%*), there was not a significant change in the VPTT (**Table 3.1, Figure 3.2a**). Incorporation of a hydrophilic, anionic comonomer is generally associated with an increase in the VPTT [126]. Indeed, for P(NIPAAm-*co*-AMPS) SN hydrogels, VPTT was observed to increase with AMPS content [117]. We likewise observed this effect for select P(NIPAAm-*co*-AMPS) SN (i.e. 1$^{st}$ networks) (**Figure 3.2b**). However, for our P(NIPAAm-*co*-AMPS)/PNIPAAm DN hydrogels, the VPTT was slightly decreased (~1 $^{o}$C for $T_{max}$) versus that of *SN-0%* and *DN-0%*, irrespective of AMPS content in the 1$^{st}$ network. Thus, the "PNIPAAm-only" 2$^{nd}$ network exhibits at PNIPAAm hydrogel-like VPTT despite the presence of a P(NIPAAm-*co*-AMPS) 1$^{st}$ network. The slightly lower VPTT values are attributed to the PNIPAAm 2$^{nd}$ networks' lower crosslink density [127].

*3.4.3. Morphology*

Hydrogel morphology was studied by SEM. Specimens were prepared with freeze-drying as this is known to preserve the structure and volume of swollen hydrogels even after all (or almost all) of the solvent is removed [128]. The pore size of DN hydrogels increased substantially as the AMPS content was increased in the 1st network

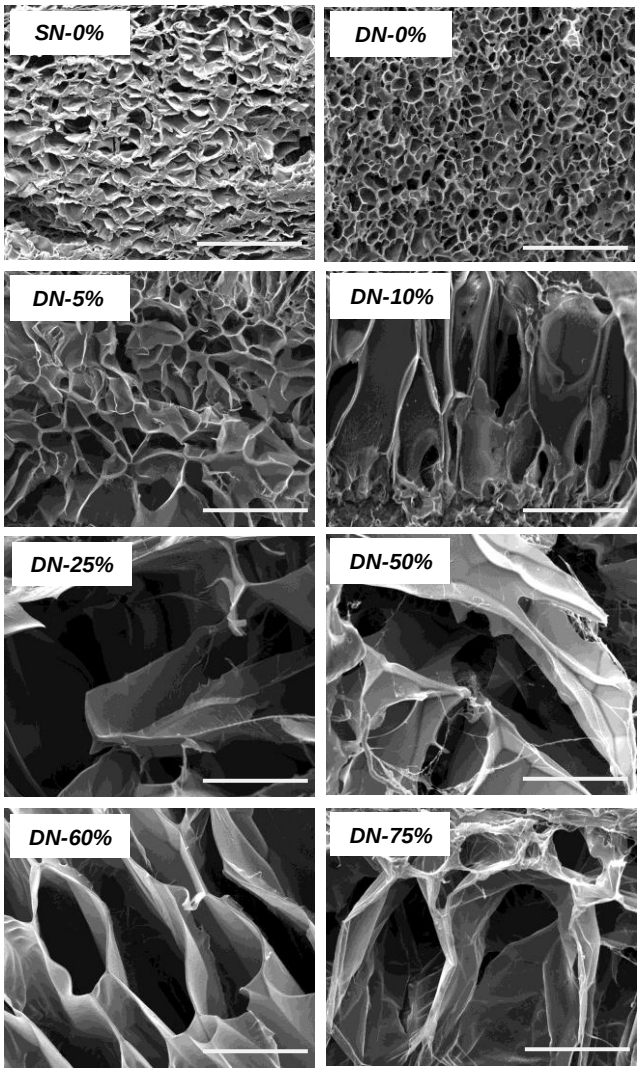


**Figure 3.3.** SEM micrographs of hydrogels. All scale bars = 50 μm.

(**Figure 3.3**). This observation is consistent with the corresponding increase in hydrogel dimension when allowed to swell in water (**Figure 3.1d**).

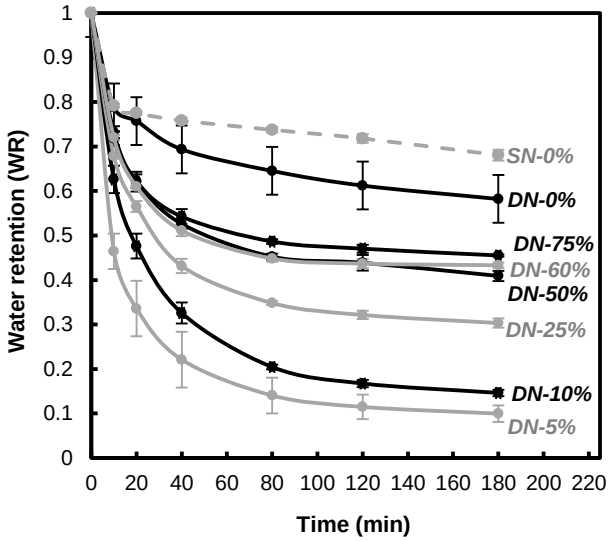


**Figure 3.4.** Hydrogel deswelling kinetics at 50 °C (by mass). All scale bars = 50 μm.

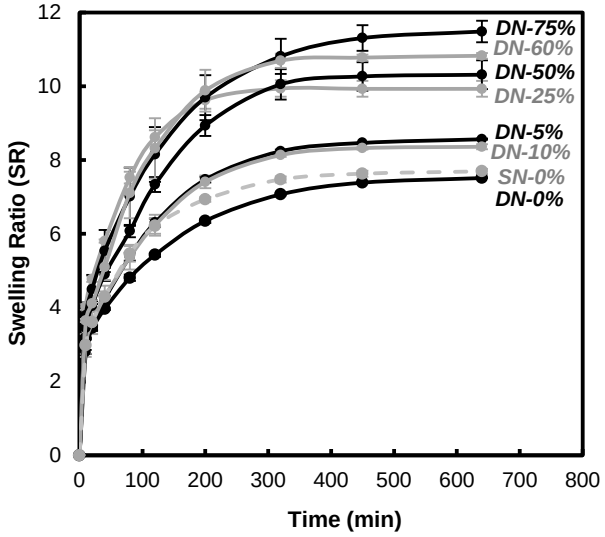


**Figure 3.5.** Hydrogel reswelling kinetics at 22 °C (by mass).

*3.4.4 Kinetic deswelling/reswelling*

For release and delivery applications, PNIPAAm-based hydrogels should exhibit a rapid and extensive response to thermal modulation (i.e. thermosensitivity). The thermosensitivity of hydrogels were determined by measuring the rate and extent to which they deswelled at 50 ºC (> VPTT) (**Figure 3.4**) and subsequently re-swelled at 22 ºC (< VPTT) (**Figure 3.5**).

*DN-0%* exhibited an enhanced rate and extent of deswelling versus *SN-0%* due to the former's asymmetrically crosslinked network structure and larger pore size which permitted a greater collapse (**Figure 3.4**) [116]. Thermosensitivity was dramatically improved for *DN-5%*. However, as AMPS levels were further increased in the 1$^{st}$ network, deswelling systematically decreased. Thus, as AMPS levels were increased (beyond a 95:5 wt% ratio of NIPAAm:AMPS), the increase in electrostatic forces appeared to inhibit the ability of the hydrogel to collapse when heated above the VPTT. Still, *DN-75%* exhibited enhanced deswelling behavior versus *SN-0%* and *DN-0%*.

When the deswollen specimens were reswollen, *DN-0%* and *SN-0%* exhibited similar thermosensitivity. As AMPS levels were systematically increased in the 1$^{st}$ network, the P(NIPAAm-*co*-AMPS)/PNIPAAm DN hydrogels exhibited an increased rate and extent of reswelling (**Figure 3.5**). In contrast to deswelling, increased electrostatic forces (i.e. increased AMPS) enhances electrostatic repulsive forces to facilitate re-expansion and reswelling of the network via an increase in osmotic pressure [124].

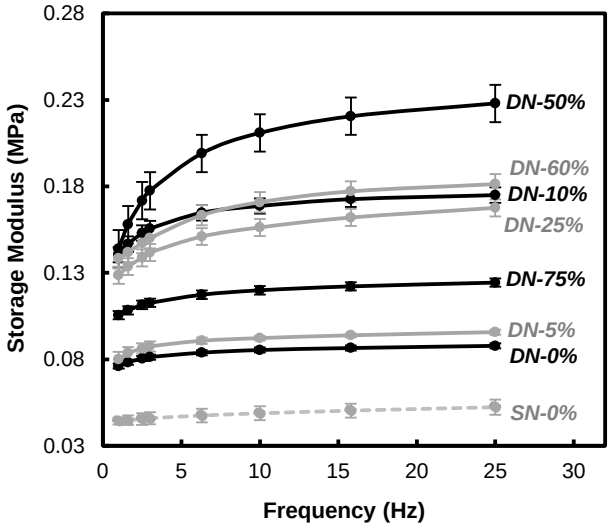


**Figure 3.6.** Storage modulus (G') of hydrogels.

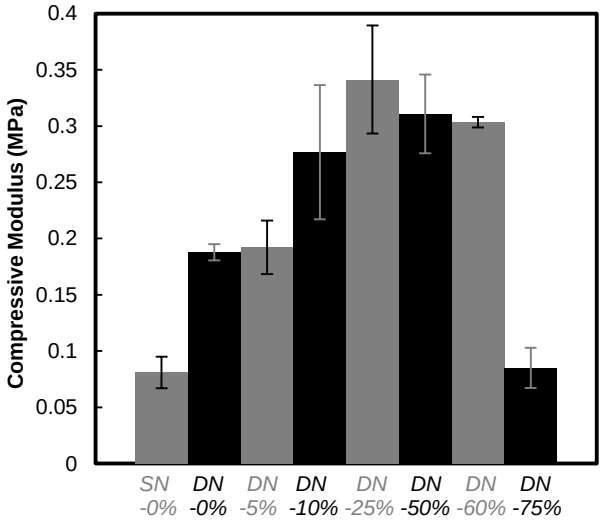


**Figure 3.7.** Compressive modulus (E) of hydrogels.

*3.4.5. Mechanical properties*

The ability of PNIPAAm-hydrogels to withstand mechanical forces both *in vitro* and *in vivo* is critical to their utility. An increase in hydrogel swelling ratio is typically associated with an decrease in strength and modulus [65]. Thus, the swelling ratio (*SR*) of the hydrogel specimen must be considered when evaluating measured mechanical properties. Here, the *SR* of specimens subjected to mechanical tests may be considered to be that recorded at time = 640 min (**Figure 3.5**).

DMA was used to measure hydrogel stiffness in terms of the storage modulus (*G'*) as a function of frequency of the applied compressive strain (**Figure 3.6**). Despite having a similar *SR*, *G'* of *DN-0%* was nearly twice that of *SN-0%* due former's asymmetrically crosslinked network [105]. *G'* generally increased as the AMPS levels were increased in the 1st network up to ~50:50 wt% ratio of NIPAAm:AMPS (i.e. *DN-50%).* However, higher levels of AMPS produced a decrease in *G'*. Likewise, during quasi-static compression tests, the compressive modulus (*E*) was observed to increase with AMPS content in the 1st network before decreasing again (**Table 3.1, Figure 3.7**). This modulus trend has also been previously observed for the P(AAm-*co*-AMPS) SN [129] and P(DMAAm-*co*-AMPS) SN [130] hydrogels. It has been proposed that, beyond a certain level of AMPS, the effective crosslink density of the network is decreased due to a high concentration of electrostatic forces (i.e. AMPS content) which produce a highly extended chain conformation [129]. This reduction in the effective crosslink density leads to a decrease in modulus. Still, the E value of ~0.3 MPa for *DN-25%* and *DN-50%* is notable and similar to that observed for PAMPS/PAAm DN hydrogels [92].

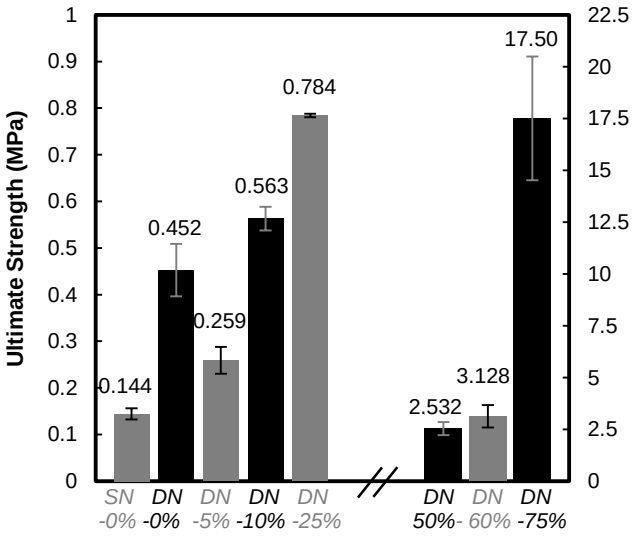


**Figure 3.8.** Ultimate compressive strength (UCS) of hydrogels.

Compression tests also were also used to measure hydrogel ultimate compressive strength (UCS) (**Table 3.1, Fig. 3.8**). UCS of *DN-0%* was over three times greater than that of *SN-0%* due former's asymmetrically crosslinked network [105]. For *DN-5%*, *UCS* decreased somewhat. However, as AMPS levels in the 1st network was increased from 90:10 to 40:60 wt% (NIPAAm:AMPS), UCS steadily increased. Most noteworthy was the exceptional UCS (~17.5 MPa) achieved by *DN-75%*. This is particularly significant given its SR of ~11.5 (i.e. a weight increase of 11.5X versus the dry state) (**Figure 3.5**). The UCS of *DN-75%* is similar to that of PAMPS/PAAm DN hydrogels (~17.2 MPa) whose strength has been attributed a 1st network which, by itself, is quite brittle, but whose crack propagation is prevented by a loosely crosslinked 2nd network which effectively dissipates stress [34, 92, 131]. The %strain at break of *DN-75%* (95%) was also the highest for this series of hydrogels.

### 3.5. Conclusions

To summarize, P(NIPAAm-*co*-AMPS)/PNIPAAm DN hydrogels were produced from a tightly crosslinked 1st network comprised of variable levels of AMPS (100:0 to 25:75 wt% ratio NIPAAm:AMPS) and a loosely crosslinked 2nd network comprised of PNIPAAm. For all of these DN hydrogels, their VPTT was only slightly decreased (~1 °C) versus the "all PNIPAAm" *SN-0%* and *DN-0%*. Thus, the 2nd PNIPAAm network effectively dominated the VPTT process. As the AMPS content increased in the 1st network, the pore size of the DN hydrogels increased substantially and produced enhanced water uptake and swollen gel dimensions. All P(NIPAAm-*co*-AMPS)/PNIPAAm DN hydrogels exhibited enhanced thermosensitivity versus *SN-0%* and *DN-0%*. While increased electrostatic repulsive forces with AMPS content resulted in a systematic reduction in the extent and rate of deswelling, re-swelling behavior was enhanced. Consistent with that observed for other polyelectrolyte networks, the modulus of P(NIPAAm-*co*-AMPS)/PNIPAAm DN hydrogels initially increased with AMPS content but then decreased. UCS steadily increased with AMPS content, reaching an impressive 17.5 MPa for *DN-75%* (i.e. 25:75 wt% NIPAAm:AMPS in the 1st network). The combined properties of the ultra-strong *DN-75%* (UCS = 17.5 MPa), including a high modulus ($E$ = 0.085 MPa) and strain at break (95%), distinguishes it from conventional thermoresponsive PNIPAAm SN hydrogels.

# CHAPTER IV

# THERMORESPONSIVE DOUBLE NETWORK MICROPILLARED HYDROGELS FOR CONTROLLED CELL RELEASE*

## 4.1. Overview

Thermoresponsive poly(*N*-isopropylacrylamide) (PNIPAAm) hydrogels have been widely used for controlled cell detachment. In this study, cell release is enhanced via deswelling with a two-pronged approach combining a double network (DN) design and micropatterning. PNIPAAm hydrogels are prepared as *DN* comprised of a tightly crosslinked 1st network and a loosely crosslinked 2nd network. Moreover, the PNIPAAm DN hydrogels are prepared as both planar 1.5 mm-thick slabs as well as micropillar arrays (~200 μm pillar diameter). Compared to the corresponding conventional single network (SN) hydrogels, DN hydrogels exhibit enhanced thermosensitivity and cell release efficiency, particularly for the micropillar arrays.

## 4.2. Introduction

Thermoresponsive poly(*N*-isopropylacrylamide) (PNIPAAm) hydrogels exhibit a reversible volume phase transition from a swollen, hydrophilic state to a deswollen, hydrophobic state when heated above its volume phase transition temperature (VPTT, ~33-35 ºC) [39, 40].

---

* Reprinted with permission from "Thermoresponsive double network micropillared hydrogels for controlled cell release" by Fei R, George JT, Park J, Grunlan MA, 2014. *Macromolecular Bioscience*, 14, 1346-52, Copyright 2014 by Wiley-VCH Verlag GmbH & Co. KGaA.

Thus, PNIPAAm hydrogels have been studied for thermally-modulated cell-release applications, including cell sheet tissue engineering [29, 132, 133], anti-fouling coatings [33, 107] and "self-cleaning membranes" for implanted biosensors [41, 62, 134]. Cell-release may occur either via a swelling [29, 33, 107, 132, 133] or deswelling-induced mechanism [41, 62, 134]. For instance, cell sheets cultured at 37 ºC (T > VPTT) were recovered without enzymatic digestion via swelling-release by lowering the temperature below the VPTT [29, 132, 133]. When designed as a membrane to permit glucose diffusion in the swollen-state, cell-release was afforded via a dewelling mechanism [41, 62, 134].

Improving the efficacy of cell-release critically rests on enhancing the thermosensitivity (i.e. rate and extent deswelling or swelling). Conventional PNIPAAm "single network" (SN) hydrogels prepared via copolymerization of *N*-isopropylacrylamide (NIPAAm) and a crosslinker such as *N*,*N*'-methylenebisacrylamide (BIS) exhibit limited thermosensitivity [70, 108]. Unfortunately, strategies to enhance thermosensitivity (without altering the VPTT) are typically associated with reduced mechanical strength and stiffness, including: heterogeneous morphologies [71-73, 112], comb-type networks [70, 135, 136] and poration [74-76, 137]. Other strategies rely on chemical modification of the PNIPAAm network to render it more hydrophilic in order to reduce the formation of a dense "skin" layer that inhibits water diffusion [138]. However, copolymerization of NIPAAm with a hydrophilic comonomer is known to increase the VPTT of the resulting hydrogel [126, 139, 140] which may be undesirable. For instance, the copolymerization of NIPAAm with 2-carboxyisopropyl acrylamide

(CIPAAm) [141, 142] as well as incorporation of poly(ethylene glycol) (PEG) grafts [143] enhanced swelling-driven cell-release but with a concomitant increase in the VPTT.

In this work, a DN hydrogel design was used to enhance thermosensitivity of PNIPAAm in order to increase cell-release via thermally-induced deswelling. A type of interpenetrating polymer network (IPN), DN hydrogels are distinguished by their asymmetrically crosslinked network [35, 90]. Reports of DN hydrogels have largely focused on systems which are non-thermoresponsive [34, 35, 91-94, 144]. While PNIPAAm IPNs have been reported and displayed enhanced mechanical properties, their swelling was diminished [96]. In contrast, we recently prepared a PNIPAAm DN hydrogel and compared their properties to the analogous SN hydrogel [116]. The VPTT of the DN hydrogel was not altered versus that of the SN hydrogel but the modulus was nearly doubled. Moreover, we observed the PNIPAAm DN hydrogel essentially maintained equilibrium swelling and reswelling kinetics, but enhanced the extent and rate of deswelling.

Herein, to further enhance thermosensitivity and deswelling-induced cell release efficiency, PNIPAAm DN hydrogels were also formed as micropillar arrays. As noted above, PNIPAAm SN hydrogels formed as mm-thick planar slabs exhibit limited thermosensitivity. While the PNIPAAm DN design improves thermosensitivity,[116] reduction of hydrogel size to the micron-scale takes advantage of the fact that kinetics of deswelling/reswelling are proportional to the square of the smallest dimension [145,

146]. Given this, PNIPAAm SN hydrogels have been prepared as micron-scale pillars and their thermosensitivity and cell-release behavior evaluated [147-150].

Herein, PNIPAAm DN hydrogels were formed with a bulk planar and micropillar arrays. Their thermosensitivity and deswelling-release of mesenchymal progenitor cells (10T1/2) was evaluated and compared to the corresponding SN hydrogels.

## 4.3. Materials and Methods

### *4.3.1. Materials*

N-isopropylacrylamide (NIPAAm, 97%) was obtained from Aldrich. N,N'-methylenebisacrylamide (BIS, 99%) was purchased from ACROS. 1-[4-(2-hydroxy)-phenyl]-2-hydroxy-2-methyl-1-propane-1-one (Irgacure 2959) was purchased from BASF. Dulbecco's modified eagle medium (DMEN), Dulbecco's phosphate-buffered solution (DPBS, pH = 7.4, without calcium and magnesium) and penicillin/streptomycin/amphotericin were obtained from Life Technologies (Carlsbad, CA). 1X Phosphate-buffered saline (PBS, pH 7.4) was obtained from Mediatech Inc. (Manassas, VA). Fetal bovine serum (FBS) was obtained from Hyclone (Logan, UT). Mesenchymal progenitor cells (10T1/2) were obtained from the American Type Culture Collection (ATCC, Manassas, VA). Lactate dehydrogenase (LDH) cytotoxicity assay kit was obtained from Pierce (Rockford, IL). Rat dermal fibroblast cells and growth medium were purchased from Cell Applications Inc. (San Diego, CA).

*4.3.2. Preparation of hydrogel aqueous precursor solutions*

SN hydrogels (including those that serve as the 1st network in DN hydrogels) were prepared via *in situ* photocure of aqueous precursor solutions containing NIPAAm monomer, BIS crosslinker, Irgacure-2959 photoinitiator and distilled (DI) water. In a 50 mL round bottom (rb) flask equipped with a Teflon-covered stir bar, NIPAAm (total weight equal to 1.0 g), BIS (0.04 g) and Irgacure (0.08 g) were dissolved in DI water (7.0 mL). DN hydrogels were prepared by soaking the SN hydrogel (i.e. the 1st network) in a solution of NIPAAm (6.0 g), BIS (0.012 g), Irgacure-2959 (0.24 g) and DI water.

*4.3.3. Preparation of SN and DN planar hydrogels*

Planar hydrogel sheets were prepared by pipetting the *SN* precursor solution into a rectangular mold formed by sandwiching polycarbonate spacers (1.5 mm thick) between two clamped glass microscope slides. The mold was submerged in an ice water bath (~7 ºC) and subjected to UV light (UV-transilluminator, 6 mW/cm$^2$, 365 nm) for 30 min. After removal from the mold, the hydrogel sheet was rinsed with DI water and then soaked in DI water for 2 days with daily water changes to remove impurities. Specimens used for analyses were taken from hydrogel sheets following soaking.

*4.3.4. Preparation of SN and DN hydrogel micropillar arrays*

SN and DN micropillars were patterned by combining photolithography and a photomask. Hydrogel micropillar arrays were formed onto glass slides (i.e. substrates) previously cleaned with Piranha solution ($H_2O_2$:$H_2SO_4$ = 1:3 v/v; WARNING: Piranha solution should be handled with extreme caution.) for 30 min followed by thorough washing with DI water and drying under a stream of $N_2$. Poly(methyl methacrylate) (PMMA) slides were cleaned with isopropanol and DI water followed by drying with $N_2$. The glass slide (top) and PMMA slide (bottom) were separated by a 180 μm thick PMMA spacer (previously cleaned with isopropanol and DI water) that defined the height of the micropillars. A photolithography mask with circular patterns (diameter: 200 μm; center to center spacing: 300 μm; total area: 3.2 $mm^2$) was placed on top of the Piranha-cleaned glass slide side of the sandwiched structure. The SN precursor solution was injected in the space between the glass slide and PMMA slide, the sandwiched structure immersed in an ice water bath (~7 ºC) for ~2 min and finally exposed to UV light (Omnicure Series 1000, 15 mW $cm^{-2}$, 365 nm; Plano, TX) for 90 sec. The spacer was removed and the glass slide with the attached SN hydrogel micropillar array was soaked in DI water.

The corresponding DN hydrogel micropillar array was prepared as follows. First, the SN micropillar array (formed onto the glass slide) was allowed to air dry (3 hr). Next, 200 μL of the DN precursor solution was delivered via syringe onto the SN micropillar array such that it was fully covered. After incubating in a humidity chamber for 1 hr, the array was thoroughly rinsed with DI water. The resulting glass slide bearing

the array structure was then covered with a PMMA slide and a spacer placed in between the two slides and exposed again with the UV light source for 90 sec (without a photomask).

*4.3.5. Imaging of hydrogel micropillar arrays*

The morphology of micropillars was studied by scanning electron microscopy (SEM). The air-dried micropillars were subjected to Pt-sputter coating and viewed with a field emission SEM (FEI Quanta 600) at accelerated electron energy of 10 keV.

*4.3.6. Temperature-modulated deswelling and reswelling*

The dynamic deswelling and reswelling of SN and DN hydrogel micropillars was quantified by measuring pillar diameter during thermal cycling. A glass substrate containing a hydrogel micropillar array was placed on top of a thermal heater with a thermal ribbon sensor (Minco Inc., Midway, TN) and temperature was regulated by a thermostat (CT16A2, Minco Inc.). Each micropillar array was carefully covered with DI water via pipette. Micropillar deswelling and reswelling was analyzed during continuous thermal cycling above and below the VPTT, respectively, as follows. After 15 min (or when the diameter of the micropillars became constant), the temperature was increased from ~26 ºC to 50 ºC at a rate of 1.02 ºC/sec and subsequently immediately cooled at a rate of 0.03 ºC/sec. Micropillar diameter was continuously recorded with a microscope (ECLIPSE LV 100D, Nikon Inc. Melville, NY) equipped with a CCD camera. Videos

were taken at a rate of 0.2 fps. Average diameters and standard deviations were calculated based on six randomly chosen pillars on each frame.

*4.3.7. Cytocompatibility*

DN hydrogel cytocompatibility was evaluated by measuring LDH concentrations released by rat dermal fibroblast cells 24 h after cell seeding versus that of cytocompatible control, tissue culture plastic (i.e. polystyrene, PS). A planar DN hydrogel sheet was prepared as described above. Three 6 mm discs were punched from the sheet and then sterilized by immersion in 80% EtOH for 45 min. The hydrogel discs were then washed 3X (30 min each) with sterile PBS, submerged in PBS for 24 hr, and subsequently transferred to a sterile 24-well plate. Next, rat dermal fibroblast cells suspended in rat fibroblast growth medium, were seeded onto each hydrogel disc and also into the empty tissue culture plastic wells at a concentration of ~6500 cells $cm^{-2}$. Cells were allowed to incubate for 24 hr at ~37 $^{o}C$ with 5% $CO_2$. Finally, the media from each well was extracted and assessed for LDH level per the manufacture's protocol. The relative LDH activity was calculated by normalizing DN sample absorption to that of PS.

*4.3.8. Cell preparation*

Cryopreserved 10T1/2 cells were thawed and expanded in monolayer culture in accordance with ATCC protocols. Until the time of harvest, the cells were maintained at

37 °C/5% $CO_2$ in DMEM supplemented with 10% heat-inactivated FBS, 100 U/mL Penicillin, 100 g/L streptomycin, and 250 μg/L amphotericin (1% PSA).

*4.3.9. Temperature-dependent cell release behavior*

SN and DN planar hydrogels and micropillar arrays were soaked in PBS (2 days) and then sterilized by sequential UV-irradiation (1 hr), soaking in 70% EtOH (1hr) and rinsing three times (15 min each) with DPBS supplemented with 1% PSA. Next, hydrogels were coated with DMEM supplemented with 40% FBS and antibiotics (PSA) for 1 hr at 30 °C (< VPTT) (i.e. hydrogel in the swollen state). Afterwards, the media was removed and 10T1/2 cells (suspended in fresh media containing 10% serum) were seeded onto each hydrogel surface at ~25,000 cells/$cm^2$ (for planar hydrogels) and ~250,000 cells/$cm^2$ (for micropillar arrays). After incubation at 30 ºC for 5 hr (for planar hydrogels) and 3 hr (for micropillar hydrogels), specimens were transferred to a Zeiss Axiovert A200 microscope (Carl Zeiss, Germany) equipped with a plate incubation chamber pre-heated to 30 °C via a temperature controller (Carl Zeiss, Germany). The chamber temperature was increased at a rate of ~2 °C/min to 35 °C (> VPTT) for planar hydrogels and 37 °C (> VPTT) for micropillars in order to induce deswelling. After

equilibration at 35 or 37 °C for 5 min, hydrogels were air-cooled at ~2 °C/min to 30 °C in order to induce reswelling. Sequential heating and cooling cycles were immediately repeated with images captured at the initial swollen (< VPTT) and final deswollen (> VPTT) states until cells were released from the hydrogel surface. For *SN* and *DN* micropillars, three different arrays of each were analyzed.

## 4.4. Results and Discussion

### *4.4.1. SEM images of SN and DN hydrogel micropillars*

The gross morphology of the micropillar arrays was evaluated by SEM (**Figure 4.1**). Both individual *SN* and *DN* micropillars (~200 μm diameter) were well-shaped and separated from each other. Perhaps due to the enhanced modulus of DN hydrogels [116], individual DN micropillars were better able retain a superior pillar shape. On average, SN and DN micropillar arrays showed similarly low occurrence of micropillar imperfections (e.g. missing pillars).

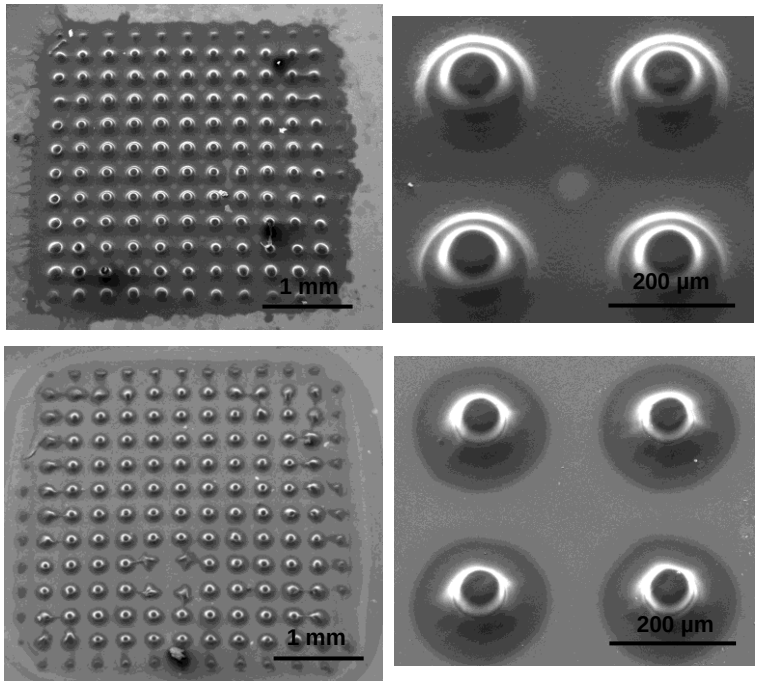


**Figure 4.1.** SEM images of SN hydrogel micropillar array (top row) and DN hydrogel micropillar array (bottom row).

*4.4.2. Temperature-modulated deswelling and reswelling*

The optically clear appearance of planar and micropillared SN and DN hydrogels is consistent with a homogeneous morphology [72, 98, 151]. In a previous report, likewise prepared SN and DN planar hydrogels (1.5 mm thick) exhibited similar VPTT values [116]. Measured by differential scanning calorimetry (DSC), the onset ($T_o$) and maximum temperature ($T_m$) endothermic peak of the VPTT values were approximately 32.2 and 34.0 ºC, respectively [116]. Versus SN planar hydrogels, planar DN hydrogels essentially maintained equilibrium swelling and reswelling kinetics but displayed an increase in the rate and extent of deswelling [116]. In this present work, the

thermosensitivity of micropillared DN hydrogels was compared to analogous SN hydrogels in terms of the rate and extent of diameter change during thermal cycling (**Figure 4.2**). Upon heating to 50 °C (> VPTT*)*, both the SN and DN micropillars decreased in diameter due to dewelling (**Figure 4.2a** and **b**, respectively). However, the DN micropillars deswelled to a greater extent (i.e. greater % shrinkage) and at a faster rate (**Figure 4.2c**). Rewelling of the DN micropillars was likewise improved. Thus, compared to the analogous SN hydrogels, the enhanced thermosensitivity observed for planar DN hydrogels [116] is also observed for DN hydrogel micropillar.

*4.4.3. Temperature-dependent cell release behavior*

The non-cytoxicity of the DN hydrogel was verfied via LDH activity assays (Supporting Information). No statistical difference in normalized levels of exogeneous LDH activity was observed for the DN hydrogel versus the tissue culture plastic.

*4.4.4. Temperature-dependent cell release behavior*

The efficacy of thermally-driven cell-release was evaluated in terms of both a

DN hydrogel design and micropatterning. Following thermal cycling, cell morphology was used as an indicator of cell attachment versus detachment. First, with respect to the DN hydrogel design strategy, cell-release from SN and DN planar hydrogels (1.5 mm thick) were compared. After seeding and incubation of cells (10T1/2) on planar hydrogels at 30 °C, the temperature was increased to 35 °C (> VPTT) to invoke deswelling and decreased back to 30 °C for reswelling. After two consecutive thermal cyles, cells on the planar SN hydrogel maintained a spread morphology, indicative of sustained attachment. (**Figure 4.3a and 4.3b**).

In contrast, cells on the planar DN hydrogel surface exhibited a round morphology indicative of end stages of detachment (**Figure 4.3d**), which is not caused by its cell compatibility (**Figure 4.4**). Our previous observations of the enhanced thermosensitivity (i.e. faster and greater volume change during deswelling/reswelling) of planar DN versus SN hydrogels is consistent these results.

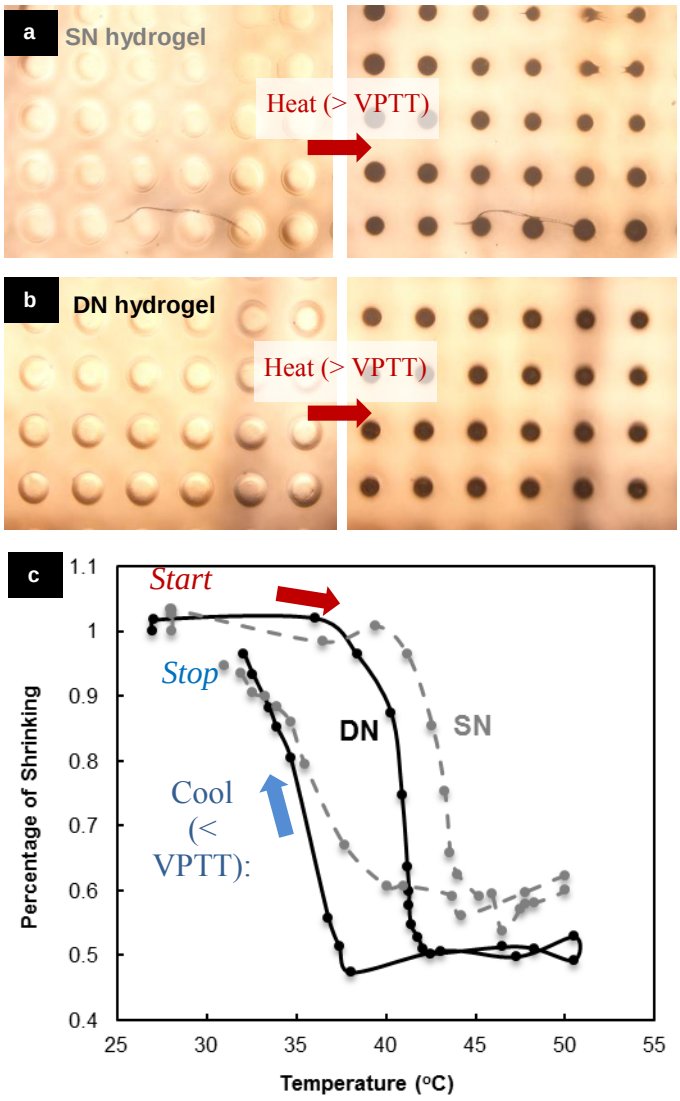


**Figure 4.2.** (a) Deswelling of SN micropillars, (b) deswelling of DN micropillars, (c) % of shrinkage (i.e. reduction of diameter) during thermal cycling.

**Table 4.1.** The number of thermal cycles for cell release

| Sample Group | $n^a_{DN}$ | $n_{SN}$ | $n_{SN}/n_{DN}$ |
|---|---|---|---|
| 1 | 3 | 5 | 1.7 |
| 2 | 5 | 7 | 1.4 |
| 3 | 5 | 9 | 1.8 |
| Average | 4.3 | 7.0 | 1.6 |

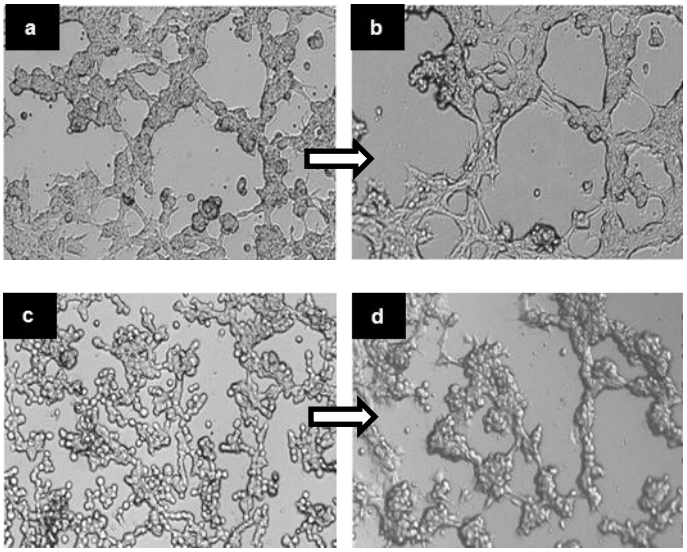


**Figure 4.3.** Deswelling-release of cells from planar (1.5 mm thick) SN and DN PNIPAAm hydrogel upon thermal cycling from 30 ºC (T < VPTT) to 35 ºC (T > VPTT) for two cycles. (a) SN at 30 ºC [1st cycle], (b) SN at 35 ºC [2nd cycle], (c) DN at 30 ºC [1st cycle], (d) DN at 35 ºC [2nd cycle]. The round morphology observed for the DN hydrogel (d) is indicative of cell detachment.

Second, the effectiveness of the micropatterning strategy was assessed by examining cell-release from micropillared SN versus DN hydrogels. After seeding and incubation, it was observed that cells attached and proliferated along the sides of and in between swollen micropillars, but not on the "tops" of the micropillars. This may result from possibly curved tops of the micropillars. Micropillar hydrogels were subjected to continuous cyclical deswelling and reswelling, respectively, by heating above and cooling below the *VPTT* until the cell sheet completely detached such that it floated across the deswollen pillars (**Figure 4.5**). The number of cycles neccessary to cause

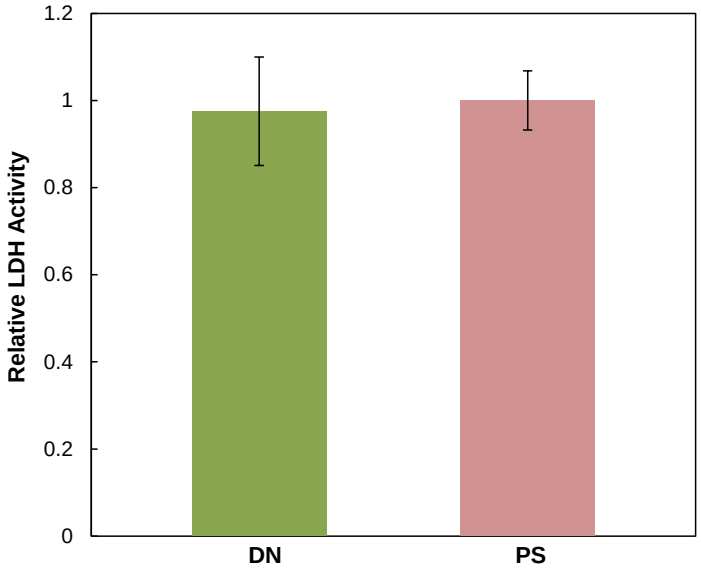


**Figure 4.4.** Relative LDH activity after 24 h for DN and polystyrene (PS) inoculated with rat dermal fibroblast cells.

detachment of the sheet was recorded based on three sample groups (i.e. 3 different micropillar arrays) (**Table 4.1**). For the case of the SN micropillars, an average of 7 thermal cycles were required to cause cell detachment (**Figure 4.5a and b**). In contrast, only an average of ~4 thermal cycles were required to detach cells from the DN micropillars (**Figure 4.5c and d**). Thus, cell detachment from DN hydrogel micropillars occured 1.6X faster versus from SN hydrogel miscropillars. The enhanced cell release of DN hydrogel micropillars is attributed to its enhanced thermosensitivity afforded by the DN.

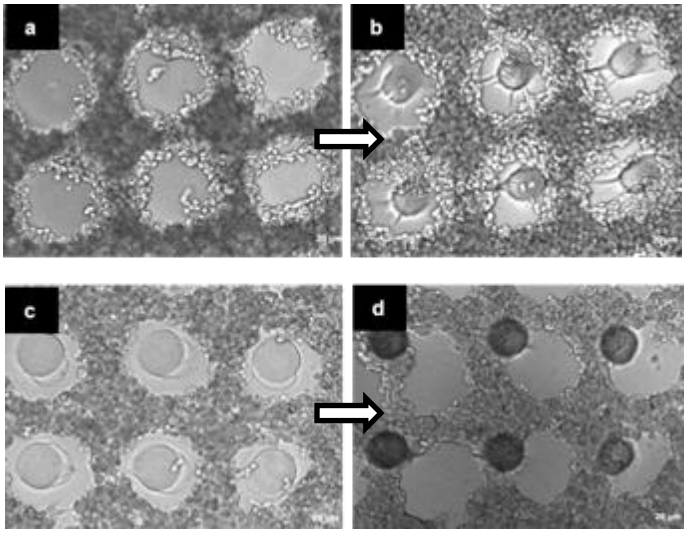


**Figure 4.5.** Deswelling-release of cells from micropillar arrays upon thermal cycling from 30 ºC (T < VPTT) to 37 ºC (T > VPTT) for multiple cycles. (a) SN at 30 ºC [1st cycle], (b) SN at 37 ºC [5th cycle], (c) DN at 30 ºC [1st cycle], (d) DN at 37 ºC [3rd cycle]. Cells floating above the pillars are considered a "complete release."

## 4.5. Conclusions

Improving the efficacy of thermally-driven cell release from PNIPAAm hydrogels is essential to realizing their potential in various applications. In this work, a two-pronged approach combining a DN design and micropatterning was employed to enhanced cell detachment from PNIPAAm hydrogels via deswelling release. Owing to the asymmetrically crosslinked, interpenetrating network structure and resulting enhanced thermosensitivity, planar (1.5 mm thick) DN hydrogels exhibited increased cell release efficiency versus analogous SN hydrogels. DN hydrogels prepared as micropillared arrays (~200 μm diameter) demonstrated enhanced thermosensitivity in terms of both the rate and extent of deswelling and reswelling when cycled above and below the VPTT, respectively. As a result, cell release was 1.6X more efficient (based on the total number of cycles required to detach the cell sheet) from DN hydrogel micropillars versus SN hydrogel micropillars.

# CHAPTER V

# P(NIPAAM-*CO*-AMPS)/PNIPAAM MEMBRANE FOR EXTENDING THE LIFETIME OF AN IMPLANTED GLUCOSE BIOSENSOR

## 5.1 Introduction

Membrane biofouling severely limits the lifetime and sensitivity of subcutaneous or transdermal glucose biosensors [7, 9]. Passive or "antifouling" membranes have largely been studied, including those based on poly(ethylene glycol)diacryalate (PEG-DA) [14], polyhydroxyethylmethacrylate (PHEMA) [21] and polytetrafluoroethylene (PTFE) [18]. Recently, our group has proposed the use of "self-cleaning membranes" based on poly(*N*-isopropylacrylamide) (PNIPAAm) hydrogels that rely on an active or "foul-releasing" mechanism to physically remove attached cells [41, 62, 134]. Thermoresponsive PNIPAAm hydrogels deswell and reswell, respectively, when heated above and cooled below their volume phase transition temperature (VPTT, ~33-35 °C) [39, 42]. Because of this behavior, PNIPAAm hydrogels have been studied for thermally-modulated, *in vitro* cell-release applications, including cell sheet tissue engineering [29, 132, 133] and anti-fouling coatings [33, 107]. To extend the utility of PNIPAAm hydrogels as self-cleaning membranes for implanted glucose biosensors, several key functional requirements must be met, including: satisfactory glucose-diffusion (for sensor functionality), thermosensitivity (for cell release) as well as robust mechanical properties (for surgical insertion and removal).

Previously, we reported a thermoresponsive PNIPAAm double network nanocomposite (DNNC) hydrogel membrane comprised of an interpenetrating, asymmetrically crosslinked PNIPAAm matrix with polysiloxane nanoparticles (~200 nm diameter) embedded during the formation of the 1st network [152]. Thermosensitivity (i.e. rate and extent of deswelling/reswelling) was improved for the DNNC hydrogel versus a conventional single network (SN) PNIPAAm hydrogel. In addition, the VPTT of the DNNC membrane was increased to ~38 °C by the inclusion of 1-2 wt% of *N*-vinylpyrrolidone (NVP) comonomer (based on NIPAAm wt) [41]. In this way, when implanted in the subcutaneous tissue of the wrist (T = 35 °C), the membrane would be swollen in the "off-state" to optimize glucose diffusion. During self-cleaning (i.e. in the "on-state"), the membrane would deswell via transdermal heating. Later, we determined glucose diffusion kinetics of the DNNC membrane as well as evaluated thermally driven *in vitro* cell release [41]. However, while the DNNC membrane was more mechanically robust versus SN PNIPAAm hydrogels [152], improved strength is expected to be valuable for membrane functionality.

More recently, we reported thermoresponsive double network (DN) hydrogels based on NIPAAm and 2-acrylamido-2-methylpropane sulfonic acid (AMPS) [116]. Gong and co-workers previously reported an ultra-strong DN hydrogel consisting of a tightly crosslinked, ionizable 1st network comprised of PAMPS and a loosely crosslinked, interpenetrating neutral 2nd network comprised of polyacrylamide (PAAm) (i.e. PAMPS/PAAm) [92]. However, while this DN system achieved exceptional strength, it is not thermoresponsive. Thus, we prepared DNs comprised of a tightly

crosslinked, ionized 1st network [P(NIPAAm-*co*-AMPS)] and a loosely crosslinked, interpenetrating 2nd network [PNIPAAm]. By incorporation of varying levels of AMPS in the 1st network (i.e. 0:100 to 75:25 wt% ratio of AMPS:NIPAAm), the thermosensitivity was improved versus that of PNIPAAm SN as well DN (i.e. no AMPS) hydrogels. Moreover, compressive strength steadily increased with AMPS content, reaching an impressive 17.5 MPa.

In this study, we evaluated the utility of P(NIPAAm-*co*-AMPS)/PNIPAAm DN hydrogels as a self-cleaning membranes for an implanted glucose biosensor. The wt% ratio of AMPS:NIPAAm was systematically increased from 0:100, 25:75, 50:50 to 75:25. To meet the specific demands of a subcutaneously implanted glucose biosensor, several critical functional properties were addressed. First, the VPTT was raised to ~38 °C with the addition 2 wt% of NVP to the 2nd network precursor solution. Second, the glucose diffusion kinetics of these membranes were experimentally measured in both the swollen and deswollen states. Third, a cylindrical membrane geometry (1.5 x 5 mm, diameter x length) thought to be suitable for implantation was used to model the glucose diffusion lag time. Finally, cylindrical membranes were used to observe the deswollen and reswollen diameter changes. Non-cytotoxicity was also confirmed. Results were compared to that of the DNNC membrane [41] and to a non-thermoresponsive PEG-DA control.

## 5.2 Materials and Methods

### *5.2.1. Materials*

*N*-isopropylacrylamide (NIPAAm, 97%), PEG-DA (MW 575 g/mol), and 1-vinyl-2-pyrrolidinone (NVP) were obtained from Aldrich. Acrylamido-2-methylpropane sulfonic acid (AMPS, 97%) and *N,N'*-methylenebisacrylamide (BIS, 99%) were purchased from ACROS. 2-Hydroxy-2-methyl-1-phenyl-1-propanone (Darocur 1173) was purchased from Ciba Specialty Chemicals (Tarrytown, NY). 1-[4-(2-Hydroxyethoxy)-phenyl]-2-hydroxy-2-methyl-1-pro-pane-1-one (Irgacure 2959) was purchased from BASF. Rat dermal fibroblast cells and growth medium were obtained from Cell Applications (San Diego, CA). Lactate dehydrogenase (LDH) cytotoxicity assay kit was obtained from Pierce (Rockford, IL). Phosphate-buffered saline (PBS, 1X , pH 7.4) was obtained from Mediatech Inc. (Manassas, VA).

### *5.2.2. Preparation of non-thermoresponsive PEG-DA hydrogels*

Precursor solutions were formed by vortexing DI-$H_2O$, PEG-DA (100%v/v), and Darocur 1173 (1% v/v) for 1 min.

Planar hydrogel sheets (~1 mm thick per electronic caliper measurements) were prepared by pipetting the precursor solution between two clamped glass slides (75 × 50 mm) separated by polycarbonate spacers (1 mm thick) and exposing the mold to longwave ultraviolet (UV) light (UVP UV-Transilluminator, 6 mW $cm^{-2}$, $\lambda$peak = 365 nm) for 30 sec at room temperature (RT). Hydrogel sheets were removed from their

molds, rinsed with DI $H_2O$, and soaked in a Petri dish containing DI $H_2O$ (60 mL) for 24 hr.

Cylindrical hydrogels (~3 mm × 5 mm, diameter × length per electronic caliper) were prepared by pipetting the precursor solution into a hollow cylindrical glass mold (inside diameter = 3.0 mm, length = 10 mm) with one end sealed by Parafilm. After sealing the other end of the mold, it was likewise exposed to longwave UV light as above at RT for 3 s. The cylindrical hydrogel was removed from the mold, rinsed with DI $H_2O$, and immersed in a Petri dish containing DI $H_2O$ (60 mL) for 24 hr. A clean razor blade was used to equally trim the ends to reduce the length to 5 mm.

*5.2.3. Preparation of thermoresponsive DN hydrogels*

DN hydrogels were prepared by sequential formation of a relatively tightly cross-linked 1st network and a loosely crosslinked 2nd network. The "1st network precursor solution" was formed with NIPAAm monomer, AMPS monomer (the wt% ratio of NIPAAm to AMPS was systematically varied), BIS crosslinker, Irgacure-2959 photo-initiator and DI water. The "2nd network precursor solution" was formed with combining NIPAAm (6.0 g), NVP (0.96 g), BIS (0.012 g), Irgacure 2959 (0.24 g), and DI $H_2O$ (21.0 g).

Planar hydrogel sheets (1 mm thick) were produced by pipetting the first network precursor solution into a mold consisting of two clamped glass slides (75 × 50 mm) separated by 0.5 or 1 mm thick polycarbonate spacers. The mold was then immersed in an ice water bath (~7 °C) and exposed to longwave UV light for 30 min. The resulting

SN P(NIPAAm-*co*-AMPS) sheet was removed from the mold, rinsed with DI $H_2O$, and then soaked in DI $H_2O$ at RT for 2 days with daily water changes. The SN sheet was then transferred into a covered Petri dish containing the 2$^{nd}$ network precursor solution for 24 hr at RT. Next, the planar hydrogel was placed into a rectangular mold (1.5 mm thick), photocured for 30 min, and finally soaked in DI $H_2O$ as above.

Cylindrical hydrogels (~3 mm × 5 mm, diameter × length) were prepared by pipetting the precursor solution into a cylindrical glass mold (inside diameter = 1 or 3 mm, length = 10 mm) as above. The mold was immersed in an ice water bath (~7 °C) and exposed for 10 min to longwave UV light. Cylindrical hydrogels were removed from their molds, rinsed with DI $H_2O$, and soaked in a Petri dish containing DI $H_2O$ (60 mL) for 2 days at RT with daily water changes. A SN cylindrical hydrogel was then transferred into a Petri dish containing the second network precursor solution for 24 hr at RT. The cylindrical hydrogel was then placed into a second cylindrical mold (diameter = ~3 mm, length = 15 mm), submerged in an ice water bath (~7 °C), exposed for 10 min to longwave UV light, and soaked in DI $H_2O$ as above. A clean razor blade was used to trim ends to reduce the cylindrical length to 5 mm.

### *5.2.4 Measurement of VPTT*

The VPTT of the P(NIPAAm-*co*-AMPS)/PNIPAAm DN hydrogels were measured with differential scanning calorimetry (DSC; TA Instruments Q100). After soaking in DI-water at RT, the hydrogel specimens were blotted with a Kim Wipe and sealed in a hermetic pan. After cooling to -50 °C, the temperature was increased to 50 °C

at a rate of 3 °C per min for 2 cycles. The resulting endothermic phase transition peak is characterized by the initial temperature at which the endotherm starts ($T_o$) and the peak temperature of the endotherm ($T_{max}$). Reported data are from the 2nd cycle.

*5.2.5. Glucose diffusion*

Planar hydrogel strips (1 cm × 1 cm × 1 mm) were placed in a side-by-side diffusion cell (PermeGear, Bethlehem, PA) positioned atop a stir plate. The donor chamber contained 3 mL of glucose solution (~1000 mg $dL^{-1}$), and the receptor chamber contained 3 mL of DI $H_2O$. Chamber solutions were stirred with Teflon-coated stir bars (800 rpm) to maintain constant solution concentrations. A water jacket maintained the designated temperature (35 and 40 °C) throughout the system. Every 10 min (for a total time of 3 h), 50 μL aliquots were removed via pipet from each chamber and glucose concentration was determined with a YSI 2700 Select Biochemistry Analyzer (YSI Incorporated, Yellow Springs, OH). The diffusion coefficients were calculated using Fick's second law of diffusion.

*5.2.6. Glucose diffusion lag time*

A computational model of the DN hydrogels was developed using COMSOL Multiphysics software (COMSOL, Inc., Los Angeles, CA). Conducting a time dependent transport of diluted species study, a geometric cylinder (3 mm × 5 mm, diameter × length) was constructed with a maximum and minimum free tetrahedral mesh element size of 0.382 and 0.0249 mm, respectively. The simulation began with a DN hydrogel

internal glucose quantity of 0 mg $dL^{-1}$ and external glucose levels of 60, 80, 160, and 300 mg $dL^{-1}$. The average glucose concentration within the cylindrical hydrogel was assessed every second for 1 hr for each external glucose concentration. The diffusion lag time was defined as the time required for the hydrogel internal glucose concentration to fall within 5% of the external glucose concentration.

### *5.2.7. Thermosensitivity*

Three cylindrical DN hydrogels (~ 3 mm × 5 mm, diameter × length) were vertically attached to a single Petri dish with a small amount of optical adhesive (Norland Optical Adhesive 61) to the base of one end. To hydrate the affixed cylinders, the Petri dish was filled with DI $H_2O$ for at least 12 hr at RT prior to thermally cycling. The Petri dish was positioned atop a heating plate under a DSLR camera (Canon Rebel T3i) with a 50 mm macro lens. Images were taken every 5 min as the hydrogels were thermally cycled between 25 and 40 °C for 5 cycles. The average rate of heating to 40 °C was ~0.7 °C/min, and passive cooling to 25 °C was ~0.22 °C/min. Thus, each cycle consisted of a 1 hr heating period followed by 1 hr of passive cooling. Cylinder diameters were analyzed by ImageJ software.

### *5.2.8. Cytocompatibility*

DN hydrogel cytocompatibility was assessed by measuring LDH concentrations released by rat dermal fibroblast cells 24 hr after cell seeding versus that of two cytocompatible controls, a PEG-DA hydrogel as well as tissue culture plastic (i.e.,

polystyrene, PS). Planar DN and PEG-DA hydrogel sheets were prepared as described above. Three 6 mm discs were punched from the sheet and then sterilized by immersion in 80% EtOH for 45 min. The hydrogel discs were then washed 3X (30 min each) with sterile PBS, submerged in PBS for 24 hr, and subsequently transferred to a sterile 24-well plate. Next, rat dermal fibroblast cells suspended in rat fibroblast growth medium, were seeded onto each hydrogel disc and also into the empty tissue culture plastic wells at a concentration of ~6500 cells $cm^{-2}$. Cells were incubated for 24 hr at ~37 °C with 5% $CO_2$. Finally, the media from each well was extracted and assessed for LDH level per the manufacture's protocol. The relative LDH activity was calculated by normalizing *DN* sample absorption to that of PS.

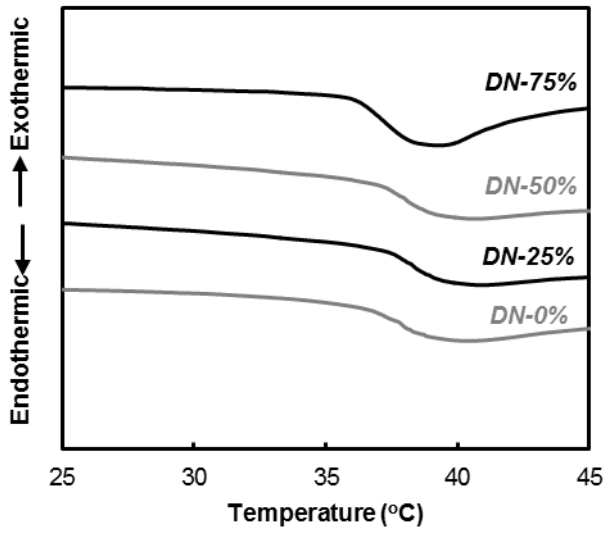


**Figure 5.1.** DSC thermograms of hydrogels

**Table 5.1.** Glucose diffusion coefficient (D) of hydrogels below and above the VPTT.

| AMPS: NIPAAm | Notation | VPTT | | 35 °C Average D ($cm^2/s$) | 40 °C Average D ($cm^2/s$) |
|---|---|---|---|---|---|
| | | $T_{\circ}$(°C) | $T_{max}$(°C) | | |
| 0:100 | *DN-0%* | 36.8 | 39.7 | $1.82 \pm 0.02 \times 10^{-6}$ | $1.16 \pm 0.02 \times 10^{-6}$ |
| 25:75 | *DN-25%* | 37.3 | 39.9 | $1.99 \pm 0.01 \times 10^{-6}$ | $0.66 \pm 0.02 \times 10^{-6}$ |
| 50:50 | *DN-50%* | 37.1 | 39.8 | $2.06 \pm 0.03 \times 10^{-6}$ | $0.75 \pm 0.01 \times 10^{-6}$ |
| 75:25 | *DN-75%* | 36.2 | 39.1 | $2.21 \pm 0.02 \times 10^{-6}$ | $1.04 \pm 0.03 \times 10^{-6}$ |

## 5.3 Results and Discussion

### *5.3.1. VPTT*

Incorporation of a hydrophilic comonomer is known to increase in the VPTT of thermoresponsive hydrogels [126]. In our previous study, the VPTT of the 1st network in the P(NIPAAm-*co*-AMPS)/PNIPAAm system was observed to increase with AMPS content [153]. Thus, the NVP comonomer was incorporated into the 2nd network precursor solution to adjust the VPTT above the subcutaneous body temperature of the wrist (~35 °C). Herein, in order to achieve a swollen "off-state" (i.e. VPTT > 35 ºC), 2% NVP (based on NIPAAm weight) was incorporated into the 2nd network. Per the DSC thermograms (**Figure 5.1**), $T_{\circ}$ and $T_{max}$ of all compositions were all close in value and greater than 35 ºC with $T_{max}$ approximately equal to ~39.6 ºC (**Table 5.1**).

### *5.3.2. Glucose diffusion*

The diffusion coefficient at 35 °C and 40 °C was assessed by examining glucose diffusion through the membrane sandwiched between side-by-side diffusion cell

**Table 5.2.** Diffusion lag times of hydrogel computational models

| Notation | Diffusion Lag Time (min) |
|---|---|
| *DN-0%* | 19.01 ± 0.22 |
| *DN-25%* | 17.29 ± 0.09 |
| *DN-50%* | 16.67 ± 0.26 |
| *DN-75%* | 15.48 ± 0.15 |

systems. Fick's 2nd law of diffusion was used to calculate the diffusion coefficients at each temperature:

$$\frac{\partial c}{\partial t} = D\frac{\partial^2 c}{\partial x^2}$$

where c is the concentration within the hydrogel, t is the time, D is the diffusion coefficient, and x is the diffusion distance [154-157]. The above equation may be modified based on the assumption that each solution preserved a uniform concentration and that each element concentration was equal at the hydrogel membrane surface as in the bulk volume of each chamber. The simplified equation is

$$Q_t = \frac{ADC_1}{L}\left(t - \frac{L^2}{6D}\right)$$

where $Q_t$ is the overall quantity of glucose transferred through the hydrogel until the specific time, t, A refers to the hydrogel area exposed to the donor or receiving chambers, $C_1$ is the initial solute concentration of the donor chamber, and L is the measured hydrogel membrane thickness.

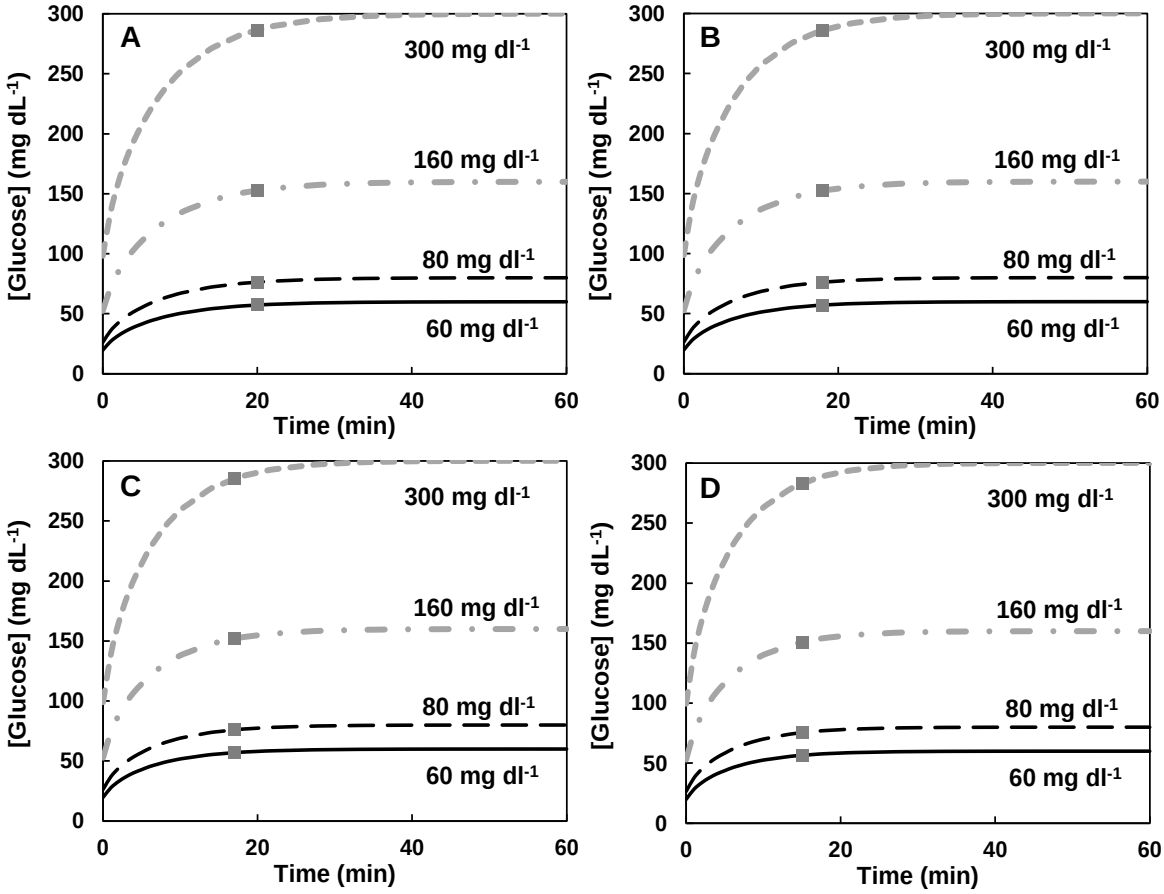


**Figure 5.2.** Computational models were utilized to determine the average glucose concentration inside cylindrical hydrogels at 35 °C for constant environment glucose levels of 60, 80, 160 and 300 mg $dL^{-1}$. Compositions of: (A) *DN-0%*; (B) *DN-25%*; (C) *DN-50%*; (D) *DN-75%*. The glucose diffusion lag time (gray■) marks when the average internal hydrogel glucose concentration is 95% to that of external environment.

The results of the study are shown in **Table 5.1**. At 35 °C (T < VPTT), the DN hydrogel membranes were at the swollen state. D of glucose through the dermis and epidermis have been reported as 2.64 ± 0.42 × $10^{-6}$ and 0.075 ± 0.05 × $10^{-6}$ $cm^2/s$, respectively [158]. Thus, the determined value of D (1.82 ± 0.02 × $10^{-6}$ $cm^2/s$) for *DN-0%* (i.e. AMPS:NIPAAm = 0:100 wt%) is within the functional range. Moreover,

glucose diffusion was similar versus a PEG-DA membrane and DNNC which were previously determined to be 1.59 ± 0.42 x $10^{-6}$ $cm^2/s$ [159] and 1.88 ± 0.01 x $10^{-6}$ $cm^2/s$ respectively [41]. As AMPS content increased, the value of D also increased which can be attributed to a more swollen membrane caused by increased electrostatic repulsion. When temperature was heated to 40 °C (T > VPTT), the membranes became deswollen. As expected, this reduced glucose diffusion as indicated by the decreased values of D. Overall, these results verify satisfactory glucose diffusion through the DN hydrogels in the "off-state". During deswelling (i.e. self-cleaning), glucose measurements would be likely prohibited.

**Table 5.3.** Max diameter for a lag time less than 5 min.

| Notation | Max Diameter (μm) |
|---|---|
| *DN-0%* | 346 |
| *DN-25%* | 394 |
| *DN-50%* | 403 |
| *DN-75%* | 417 |

A COMSOL Multiphysics computational model was utilized to determine the glucose diffusion lag time for the DN cylindrical hydrogels (diameter 1.5 mm, length 5 mm). The simulation utilized an initial glucose quantity within the hydrogel was set to 0 mg $dL^{-1}$. Subsequently, four different glucose concentrations (60, 80, 160, and 300 mg $dL^{-1}$) that represent low, normal, high and very high physiologically glucose levels [160] were applied to the cylinders. With these conditions, the average glucose concentration within the hydrogel cavity every second up to 1 hr was calculated (**Figure 5.2**). For *DN-0%* hydrogel, an average lag time of 19.01 ± 0.22 min was observed, which is similar to the *DNNC [41]*. However, as AMPS levels were increased, lag time systematically decreased and the lag time of *DN-75%* was reduced to 15.48 ± 0.15 min (**Table 5.2**). The increase in pore size and hydration may be responsible for the reduction in lag time [153]. Physiological lag times upward of 15 min have been reported between glucose changes in the interstitial fluid (ISF) and in the blood [161-165]. To further reduce the lag time, the cylinder diameter may be reduced. If a lag time of less than 5 min is targeted, the maximum diameters for DN hydrogels are shown in **Table 5.3**.

### *5.2.3. Thermosensitivity*

The extent and rate at which the cylindrical hydrogel deswells and reswells upon cyclically heating (T > VPTT) and cooling (T < VPTT) is critical for its ability to function as a self-cleaning membrane [38, 166]. The thermosensitivity of hydrogels were

determined by measuring the diameter change during thermal cycling. The diameter of a vertically affixed charged DN hydrogel (*DN-25%*, 50%, and *75%*) cylinders showed more dramatic diameter change at 40 °C compared to pure *DN-0%*. *DN-75%* exhibited a greater extent of diameter change versus *DNNC* (**Table 5.4**). After cooling to 25 °C for a period of 1 hr, the diameters of specimens all returned to within 95% of its initial measured swollen state. The reversible thermo-transition was confirmed by cyclical heating (~0.70 °C/min) and cooling (~0.22 °C/min) over a 10 hr period (**Figure 5.3**). A consistent change in diameter during each cycle was observed.

**Table 5.4.** Diameter decrease from swollen to deswollen state.

| Notation | Max Diameter Change (%) |
|---|---|
| *PEG* | N/A |
| *DNNC* | 24.8 ± 0.7 |
| *DN-0%* | 22.7 ± 2.1 |
| *DN-25%* | 24.7 ± 1.7 |
| *DN-50%* | 25.2 ± 1.7 |
| *DN-75%* | 33.2 ± 1.0 |

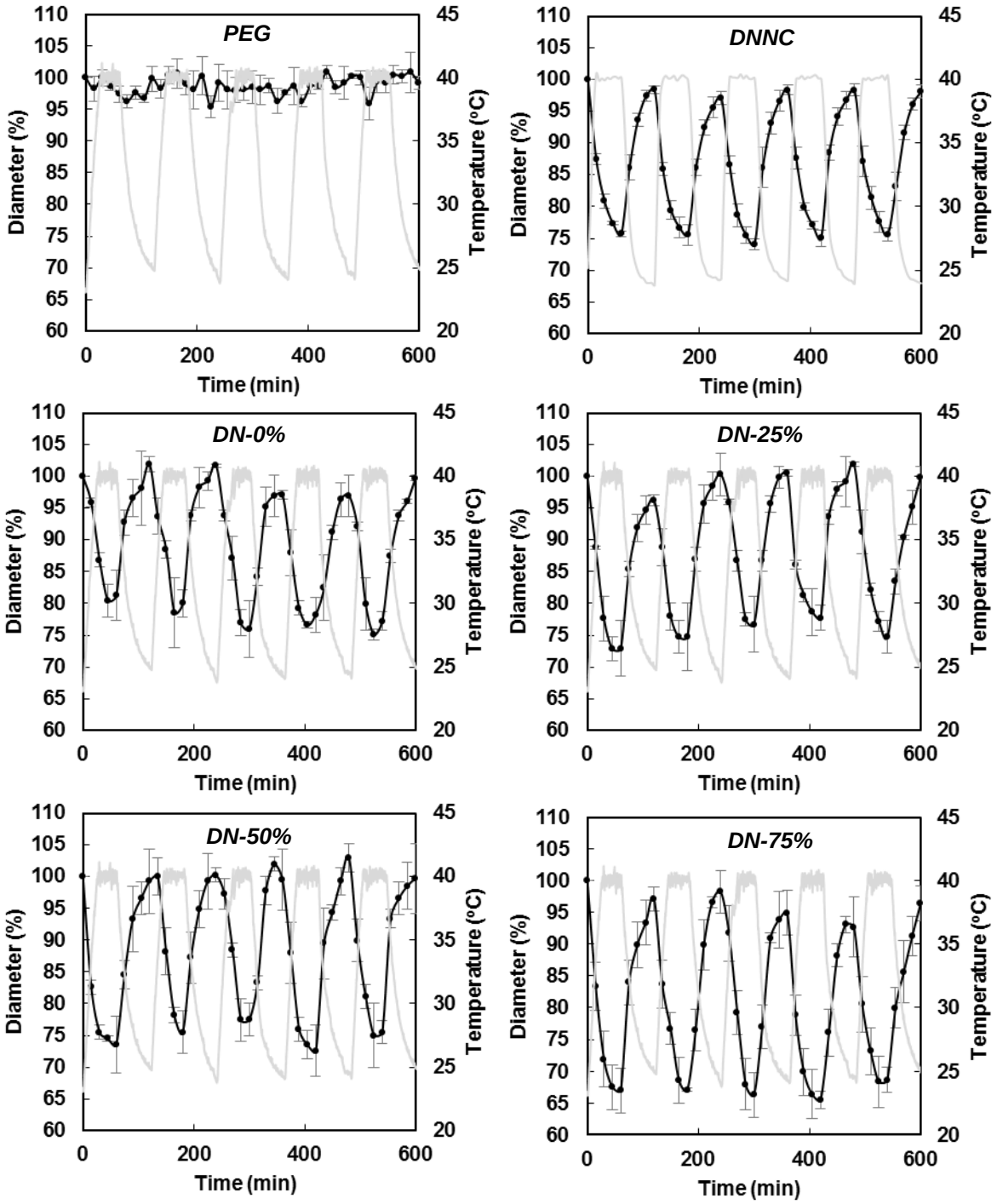


**Figure 5.3.** Diameter change during thermal cycling of a vertically affixed hydrogel cylinder over a 10 hr time period. Diameter change (blue) and temperature change (gray).

*5.3.4. Cytocompatibility*

Good cytocompatibility is an essential prerequisite for a subcutaneously implanted self-cleaning membrane to be applied in clinic. The cytocompatibility of the hydrogels was assessed via lactate dehydrogenase (LDH) activity assays. LDH is a biomarker released during tissue damage, thus can be measured to determine cellular toxicity[167]. LDH levels of different specimens released by rat dermal fibroblast cells 24 hr postseeding were analyzed. Compared to the LDH levels of non-cytotoxic PEG-DA hydrogel and tissue culture plastic (i.e. PS), All of the P(NIPAAm-*co*-AMPS)/PNIPAAm membranes exhibited similar values, which indicate low cytotoxicity toward fibroblast cells (**Figure 5.4**).

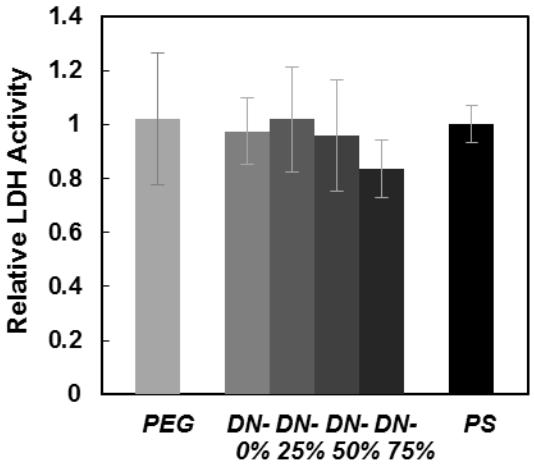


**Figure 5.4.** Relative LDH activity after 24 hr for PEG-DA, P(NIPAAm-*co*-AMPS)/PNIPAAM, and polystyrene (PS).

## 5.4 Conclusions

A thermoresponsive double network hydrogel was prepared by introduction of an electrostatic comonomer AMPS (25, 50, and 75 wt% ratio AMPS:NIPAAM) during formation of the 1st network. Its ability to function as a self-cleaning membrane for a subcutaneously implanted glucose biosensor was evaluated and compared with non-charged *DN-0%* and previously reported *DNNC*.

The VPTT was adjusted to ~38 °C with NVP comonomer to ensure that the membrane hydrated at body temperature (35 °C, temperature of wrist subcutaneous tissue) to allow sufficient glucose diffusion. At 35 °C, as the AMPS content increased in the 1st network, the glucose diffusion coefficient (D) increased due to larger pore size of the DN hydrogels. According to the prediction of a finite element model, glucose diffusion lag time for the hydrogel cylinder was further reduced. If a thinner hydrogel can be produced, the lag time is 5 min and it would be negligible compared to the glucose changes in the ISF. Compared to nanocomposite (*DNNC*) membrane, *DN-75%* electrostatic membrane exhibited faster glucose diffusion and shorter lag time.

All P(NIPAAm-*co*-AMPS)/PNIPAAm DN hydrogels exhibited enhanced thermosensitivity and greater changes in diameter were observed during thermal cycling *versus DN-0%*. Over a 10 hr period of thermal cycling, all hydrogels shown consistent reversible size change (5% of the original swollen diameter). Like the LDH results of PEG and PS, all compositions exhibited negative cytotoxicity.

# CHAPTER VI

# CONCLUSIONS AND FUTURE DIRECTION

## 6.1 Conclusions

Herein, a self-cleaning membrane for extending the lifetime of an implanted biosensor has been developed based on two thermoresponsive PNIPAAm DN hydrogel designs as well as considerations of membrane geometry and size. This active approach to control membrane biofouling is a departure from most strategies that rely on a passive mechanism which have been met with limited success. In addition, while thermally-driven *in vitro* cell release from PNIPAAm SN hydrogels has been studied, this research is the first (to our knowledge) to use PNIPAAm-based hydrogels for *in vivo* cell release. The PNIPAAm DN hydrogel systems described were carefully designed to meet the functional requirements of a self-cleaning membrane.

In Chapter II, a series of PNIPAAm DN nanocomposite hydrogels were prepared by incorporation of polysiloxane nanoparticles (~50 nm and ~200 nm) during the formation of either the 1$^{st}$ or 2$^{nd}$ network. The VPTT values were conveniently maintained at that of PNIPAAm SN hydrogels. However, the rate and extent of deswelling was enhanced, even for the DN hydrogel containing no nanoparticles. Notable, the composition based on inclusion of ~200 nm polysiloxane nanoparticles in the 1$^{st}$ network exhibited the most notable properties. For this DN nanocomposite hydrogel, equilibrium swelling was dramatically enhanced as well as deswelling–

reswelling kinetics. Despite higher equilibrium swelling at RT, its modulus and strength values exceeded that of the SN hydrogel.

In Chapter III, a series of PNIPAAm DN hydrogels containing AMPS (an electrostatic comonomer) were explored as an alternative design in order to improve mechanical properties and optical transparency. AMPS was introduced at varying levels during the formation of the 1$^{st}$, tightly crosslinked network only as this was found to maintain the VPTT values at that of PNIPAAm SN hydrogels. The highly negatively charged 1$^{st}$ network impacted several properties. Pore size and water uptake increased with AMPS content, resulting in increased swelling. While the rate and extent of deswelling was improved versus SN and DN hydrogels (i.e. no AMPS), increased AMPS content reduced this behavior. In contrast, increased AMPS content improved reswelling. The DN hydrogel containing the highest level of AMPS (i.e. 25:75 wt% NIPAAm:AMPS) exhibited exceptional ultimate strength (17.5 MPa) despite its high hydration.

In Chapter IV, the impact of combining a micron-scale dimensions and a DN design on thermally-driven cell-release was evaluated. Micropillars (~200 μm) along with analogous mm-thick planar slabs were prepared from PNIPAAm DN as well as SN compositions. Given the expected implantation of cylindrical self-cleaning membranes, cell release from a micropillar hydrogel was important to assess. Cell-release efficiency was improved for both planar and, particularly, for micropillared DN hydrogels versus analogous SN hydrogels. This correlated to the observed increase in thermally-driven change in pillar diameter for DN micropillars. As a result, cell release was 1.6X more

efficient (based on the total number of cycles required to detach the cell sheet) from DN hydrogel micropillars versus SN hydrogel micropillars.

Finally, in Chapter V, the electrostatic PNIPAAm-*co*-AMPS DN membrane design (from Chapter III) was evaluated in terms of tailoring them to meet specific functional requirements for a self-cleaning membrane for an implanted glucose biosensor. The VPTT was adjusted to ~38 °C with NVP such that the membrane would be swollen in the "off-state". Glucose diffusion increased with AMPS content in the 1$^{st}$ network and glucose diffusion lag time was reduced to ~15 min. In addition, enhanced thermosensitivity was observed as AMPS content increased and the cytocompatibility of the PNIPAAm-*co*-AMPS DN hydrogels was confirmed.

### 6.2 Future Directions

Given the results of this work, several major items remain highly relevant for future studies. First, *in vitro* and *in vivo* "self-cleaning" assessment of the PNIPAAm-*co*-AMPS DN membrane design (Chapter V) is important. In this way, the electrostatic membranes may be distinguished versus the PNIPAAm DN nanocomposite design which was previously evaluated. It is expected, due to the electrostatic forces and enhanced hydration, that *in vitro* cell release will be improved. The next step would be to select a specific membrane composition for *in vivo* studies using a subcutaneous rat model and self-cleaning behavior analyzed via histology.

In addition to assessing self-cleaning, other factors must be considered when combining with a particular glucose sensing material to form the biosensor. First,

housing of a glucose sensing material must be considered. Second, the size of the final implant and membrane thickness must also be evaluated. Of particular interest to our group is the incorporation of a fluorescent glucose sensing assay developed by Gerard Coté and co-workers which is based on the competitive binding between Alexa 647-concanavalin A (ConA) and competing ligand (aminopyrene trisulfonatemanno-tetraose, APTS-trimannose). Considerations will have to be made to incorporate the assay into the membrane to minimize leakage of the assay as well as glucose diffusion lag time (**Figure 6.1a**). A hollow cylindrical membrane may obtain these goals. However, since glucose diffusion lag time is critically associated with the size of membrane, the cylinder must also have a narrow diameter. In our studies, we noted that for the DN nanocomposite design (i.e. ~200 nm polysiloxane nanoparticles incorporated into the 1$^{st}$ network), the cylinder diameter needed to be reduced to ~350 μm to achieve a glucose diffusion lag time of ~ 5 min. For the PNIPAAm-*co*-AMPS DN membrane with the highest AMPS content, due to its faster glucose diffusion, a diameter of ~420 μm could be utilized. While we have shown our ability to fabricate hollow cylindrical membranes with inner and outer diameters of 800 and 1000 μm (**Figure 6.1b & 6.1c**), respectively, smaller dimensions are required. Thus, a major focus will be placed on new fabrication method for miniaturized DN hydrogel hollow, and possibly solid, rods. Customized mold and 3D printing technology are two potential solutions. Based on their superior optical transparency (essential for optical sensing methods), as well as better mechanical properties, enhanced thermosensitivity and superior glucose diffusion. Furthermore, their

negatively charged nature may inhibit leakage of the aforementioned assay which is also negatively charged.

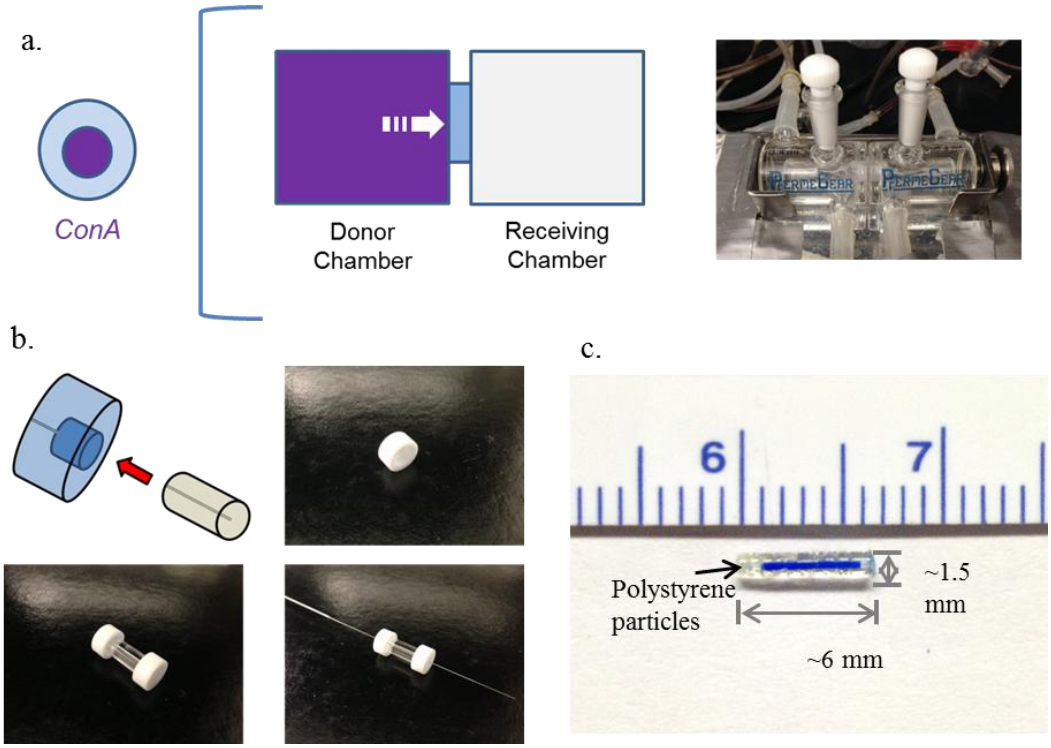


**Figure 6.1. a)** Diffusion apparatus of glucose competitive binding protein ConA against hydrogel membrane. **b)** Current fabrication method for hollow rod hydrogel. **c)** Dark blue polystyrene particles (~3 μm) ("glucose assay mimic") were injected into the inner hollow space of the hydrogel.

REFERENCES

[1] Wild S, Roglic G, Green A, Sicree R, King H. Global prevalance of diabetes. Diabetes Care. 2004;27:1047-53.

[2] World Health Organization (WHO) Fact Sheet.No. 312. http://www.who.int/mediacentre/factssheets/fs312/en/

[3] American Diabetes Association. Economic costs of diabetes in the US in 2012. Diabetes Care. 2013;36:1033-46.

[4] Shamoon H, Duffy H, Fleischer N, Engel S, Saenger P, Strelzyn M, et al. The effect of intensive treatment of diabetes on the development and progression of long-term complications in insulin-dependent diabetes mellitus. N Engl J Med. 1993;329:977-86.

[5] Nathan D, Cleary P, Backlund J, Genuth S, Lachin J, Orchard T, et al. Intensive diabetes treatment and cardiovascular disease in patients with type 1 diabetes. N Engl J Med. 2005;353:2643-53.

[6] Hovorka R. Continuous glucose monitoring and closed-loop systems. Diabetic Med. 2006;23:1-12.

[7] Group Juvenile Diabetes Research Foundation. The effect of continuous glucose monitoring in well-controlled type 1 diabetes. Diabetes Care. 2009;32:1378-83.

[8] Frost M, Meyerhoff ME. *In vivo* chemical sensors: tackling biocompatibility. Anal Chem. 2006;78:7370-7.

[9] Wisniewski N, Reichert M. Methods for reducing biosensor membrane biofouling. Colloids Surf, B. 2000;18:197-219.

[10] Anderson JM. Biological responses to materials. Annu Rev Mater Res. 2001;31:81-110.

[11] Ziats NP, Miller KM, Anderson JM. *In vitro* and *in vivo* interactions of cells with biomaterials. Biomaterials. 1988;9:5-13.

[12] Jackson JR, Seed M, Kircher C, Willoughby D, Winkler J. The codependence of angiogenesis and chronic inflammation. The FASEB Journal. 1997;11:457-65.

[13] Anderson JM, Rodriguez A, Chang DT. Foreign body reaction to biomaterials. Semin Immunol. 2008;20:86-100.

[14] Quinn CA, Connor RE, Heller A. Biocompatible, glucose-permeable hydrogel for in situ coating of implantable biosensors. Biomaterials. 1997;18:1665-70.

[15] Reuben BG, Perl O, Morgan NL, Stratford P, Dudley LY, Hawes C. Phospholipid coatings for the prevention of membrane fouling. J Chem Technol Biotechnol. 1995;63:85-91.

[16] Yang W, Xue H, Carr LR, Wang J, Jiang S. Zwitterionic poly (carboxybetaine) hydrogels for glucose biosensors in complex media. Biosens Bioelectron. 2011;26:2454-9.

[17] Brauker JH, Carr-Brendel VE, Martinson LA, Crudele J, Johnston WD, Johnson RC. Neovascularization of synthetic membranes directed by membrane microarchitecture. J Biomed Mater Res. 1995;29:1517-24.

[18] Bota P, Collie A, Puolakkainen P, Vernon RB, Sage EH, Ratner BD, et al. Biomaterial topography alters healing *in vivo* and monocyte/macrophage activation *in vitro*. J Biomed Mater Res Part A. 2010;95:649-57.

[19] Updike SJ, Shults MC, Gilligan BJ, Rhodes RK. A subcutaneous glucose sensor with improved longevity, dynamic range, and stability of calibration. Diabetes Care. 2000;23:208-14.

[20] Sharkawy AA, Klitzman B, Truskey GA, Reichert WM. Engineering the tissue which encapsulates subcutaneous implants. I. Diffusion properties. J Biomed Mater Res. 1997;37:401-12.

[21] Marshall A, Ratner B. Quantitative characterization of sphere-templated porous biomaterials. AIChE J. 2005;51:1221-32.

[22] Koschwanez H, Yap F, Klitzman B, Reichert W. *In vitro* and *in vivo* characterization of porous poly-L-lactic acid coatings for subcutaneously implanted glucose sensors. J Biomed Mater Res Part A. 2008;87:792-807.

[23] Gifford R, Batchelor MM, Lee Y, Gokulrangan G, Meyerhoff ME, Wilson GS. Mediation of*in vivo* glucose sensor inflammatory response via nitric oxide release. J Biomed Mater Res Part A. 2005;75:755-66.

[24] Frost MC, Batchelor MM, Lee Y, Zhang H, Kang Y, Oh B, et al. Preparation and characterization of implantable sensors with nitric oxide release coatings. Microchem J. 2003;74:277-88.

[25] Bhardwaj U, Sura R, Papadimitrakopoulos F, Burgess DJ. PLGA/PVA hydrogel composites for long-term inflammation control following sc implantation. Int J Pharm. 2010;384:78-86.

[26] Ward WK, Wood MD, Casey HM, Quinn MJ, Federiuk IF. The effect of local subcutaneous delivery of vascular endothelial growth factor on the function of a

chronically implanted amperometric glucose sensor. Diabetes Technol Ther. 2004;6:137-45.

[27] Collier TO, Anderson JM, Kikuchi A, Okano T. Adhesion behavior of monocytes, macrophages, and foreign body giant cells on poly (*N*-isopropylacrylamide) temperature responsive surfaces. J Biomed Mater Res. 2002;59:136-43.

[28] Kumar A, Srivastava A, Galaev IY, Mattiasson B. Smart polymers: physical forms and bioengineering applications. Prog Polym Sci. 2007;32:1205-37.

[29] Kobayashi J, Okano T. Fabrication of a thermoresponsive cell culture dish: A key technology for cell sheet tissue engineering. Sci Tech Adv Mater. 2010;11:1-12.

[30] Yamato M, Akiyama Y, Kobayashi J, Yang J, Kikuchi A, Okano T. Temperature-responsive cell culture surfaces for regenerative medicine with cell sheet engineering. Prog Polym Sci. 2007;32:1123-33.

[31] Callewaert M, Rouxhet PG, Boulangé-Petermann L. Modifying stainless steel surfaces with responsive polymers: effect of PS-PAA and PNIPAAM on cell adhesion and oil removal. J Adhes Sci Technol. 2005;19:765-81.

[32] Cunliffe D, Smart C, Tsibouklis J, Young S, Alexander C, Vulfson E. Bacterial adsorption to thermoresponsive polymer surfaces. Biotechnol Lett. 2000;22:141-5.

[33] Ista LK, López GP. Lower critical solubility temperature materials as biofouling release agents. J Ind Microbiol Biot. 1998;20:121-5.

[34] Gong JP. Why are double network hydrogels so tough? Soft Matter. 2010;6:2583-90.

[35] Myung D, Waters D, Wiseman M, Duhamel P-E, Noolandi J, Ta CN, et al. Progress in the development of interpentrating polymer networks. Polym Adv Tech. 2008;19:647-57.

[36] Haque MA, Kurokawa T, Gong JP. Super tough double network hydrogels and their application as biomaterials. Polymer. 2012;53:1805-22.

[37] Zhang X-Z, Wu D-Q, Chu C-C. Synthesis, characterization and controlled drug release of thermosensitive IPN–PNIPAAm hydrogels. Biomaterials. 2004;25:3793-805.

[38] Hou Y, Matthews AR, Smitherman AM, Bulick AS, Hahn M, Hou H, et al. Thermoresponsive nanocomposite hydrogels with cell-releasing behavior. Biomaterials. 2008;29:3175-84.

[39] Liu F, Urban MW. Recent advances and challenges in designing stimuli-responsive hydrogels. Prog Polym Sci. 2010;35:3-23.

[40] Wu XS, Hoffman AS, Yager P. Synthesis and characterization of thermally reversible macroporous poly (*N*-isopropylacrylamide) hydrogels. J Polym Sci Part A: Polym Chem. 1992;30:2121-9.

[41] Abraham AA, Fei R, Cote GL, Grunlan MA. Self-cleaning membrane to extend the lifetime of an implanted glucose biosensor. ACS Appl Mater & Interfaces. 2013;5:12832-8.

[42] Wu XS, Hoffman AS, Yager P. Synthesis and characterization of thermally reversible macroporous poly(*N*-isopropylacrylamide) hydrogels. J Polym Sci Part A: Polym Chem. 1992;30:2121-9.

[43] Hirokawa Y, Tanaka T. Volume phase transition in a nonionic gel. J Chem Phys. 1984;81:9379-80.

[44] Hoffman AS, Afrassiabi A, Dong LC. Thermally reversible hydrogels: II. delivery and selective removal of substances from aqueous solution. J Controlled Release. 1986;4:213-22.

[45] Zhang J, Pelton R, Deng Y. Temperature-dependent contact angles of water on poly(*N*-isopropylacrylamide) gels. Langmuir. 1995;11:2301-2.

[46] Chaterji S, Kwon K, Park K. Smart polymeric gels: redefining the limits of biomedical devices. Prog Polym Sci. 2007;32:1083-122.

[47] Kumar A, Srivastava A, Galaev IY, Mattiasson B. Smart polymers: physical forms and bioengineering applications. Prog Polym Sci. 2007;32:1205-37.

[48] Eddington DT, Beebe DJ. Flow control with hydrogels. Adv Drug Deliv Rev. 2004;56:199-210.

[49] Harmon ME, Tang M, Frank CW. A microfluidic actuator based on thermoresponsive hydrogels. Polymer. 2003;44:4547-56.

[50] Li Z, He Q, Ma D, Chen H. On-chip integrated multi-thermo-actuated microvalves of poly(*N*-isopropylacrylamide) for microflow injection analysis. Anal Chimica Acta. 2010;665:107-12.

[51] Freitas RFS, Cussler EL. Temperature sensitive gels as size selective absorbents. Sep Sci Tech. 1987;22:911-9.

[52] Zhiming L, Qiaohong H, Dan M, Hengwu C, A SS. Thermoswitchable electrokinetic ion-enrichment/elution based on a poly(*N*-isopropylacrylamide) hydrogel plug in a microchannel. Anal Chem. 2010;82:10030-6.

[53] Chilkoti A, Dreher MR, Meyer DE, Raucher D. Targeted drug delivery by thermally responsive polymers. Adv Drug Deliv Rev. 2002;54:613-30.

[54] Nakayama M. Thermoresponsive polymeric materials for drug delivery systems. Drug Delivery Sys. 2008;23:627-36.

[55] Qiu Y, Park K. Environment-sensitive hydrogels for drug delivery. Adv Drug Deliv Rev. 2001;53:321-9.

[56] Yamato M, Akiyama Y, Kobayashi J, Yang J, Kikuchi A, Okano T. Temperature-responsive cell culture surfaces for regenerative medicine with cell sheet engineering. Prog Polym Sci. 2007;32:1123-33.

[57] Callwaert M, Rouxhet PG, Boulange-Petermann L. Modifying stainless steel surfaces with responsive polymers: effect of PS-PAA and PNIPAAM on cell adheshion and oil removal. J Adhesion Sci Technol. 2005;19:765-81.

[58] Cunliffe D, Smart CA, Tsibouklis J, Young S, Alexander C, Vulfson EN. Bacterial adsorption to thermoresponsive polymer surfaces. Biotechnol Lett. 2000;22:141-5.

[59] Ista L, Lopez G. Lower critical solubility temperature materials as biofouling release agents. J Indust Mircrobiol Biotech. 1998;20:121-5.

[60] Chen J, Yoshida M, Maekawa Y, Tsubokawa N. Temperature-switchable vapor sensor materials based on *N*-isopropylacrylamide and calcium chloride. Polymer. 2001;42:9361-5.

[61] Gant R, Abraham A, Hou Y, Grunlan MA, Cote GL. Design of a self-cleaning thermoresponsive nanocomposite hydrogel membrane for implantable biosensors. Acta Biomaterialia. 2010;6:2903-010.

[62] Gant R, Hou Y, Grunlan MA, Cote GL. Development of a self-cleaning sensor membrane for implantable biosensors. J Biomed Mater Res. 2009;90A:695-701.

[63] Guenther M, Gerlach G, Kuckling D, Kretschmer K, Corten C, Weber J, et al. Chemical sensors based on temperature-responsive hydrogels. Proc SPIE Int Soc Opt Eng. 2006;6167:61670T/1-T/11.

[64] Zhang X-Z, Xu X-D, Cheng S-X, Zhuo R-X. Stragegies to improve the response rate of thermosensitive PNIPAAm hydrogels. Soft Matter. 2008;4:385-91.

[65] Anseth KS, Bowman CN, Brannon-Peppas L. Mechanical properties of hydrogels and their experimental determination. Biomaterials. 1995;17:1647-57.

[66] Xue W, Champ S, Huglin MB. Network and swelling parameters of chemically crosslinked thermoreversible hydrogels. Polymer. 2001;42:3665-9.

[67] Zeng K, Wang L, Zheng S. Rapid deswelling and reswelling response of poly(*N*-isopropylacrylamide) hydrogels via formation of interpenetrating polymer networks with polyhedral oligomeric silsequioxane-capped poly(ethylene oxide) amphiphilic telechelics. J Phys Chem B. 2009;113:11831-40.

[68] Liu Q, Zhang P, Qing A, Lan Y, Shi J, Lu M. Synthesis of rapid responsive gels comprising hydrophilic backbone and poly(*N*-isopropylacrylamide) graft chains by RAFT polymerization and end-linking processes. Polymer. 2006;47:6963-9.

[69] Matsuura T, Sugiyama M, Annaka M, Hara Y, Okano T. Microscopic implications of rapid shrinking of comb-type grafted poly(*N*-isopropylacrylamide) hydrogels. Polymer. 2003;44:4405-9.

[70] Yoshida R, Uchida K, Kaneko Y, Sakai K, Kikuchi A, Sakurai Y, et al. Comb-type grafted hydrogels with rapid de-swelling response to temperature changes. Nature. 1995;374:240-2.

[71] Xue W, Champ S, Huglin MB, Jones TGJ. Rapid swelling and deswelling in cryogels of crosslinked poly(*N*-isopropylacrylamide-co-acrylic). Europ Polym J. 2004;40:703-12.

[72] Yan Q, Hoffman AS. Synthesis of macroporous hydrogels with rapid swelling and deswelling properties for delivery of macromolecules. Polymer. 1995;36:887-9.

[73] Zhang X-H, Yang Y-Y, Chung T-S. The influence of cold treatment on the properties of temeprature-sensitive poly(*N*-isopropylacrylamide) hydrogels. J Coll Interface Sci. 2002;246:105-11.

[74] Serizawa T, Uemura M, Kaneko T, Akashi M. Rapid and controlled deswelling of porous poly(*N*-isopropylacrylamide) hydrogels prepared by the templating of interpenetrated nanoporous silica particles. J Polym Sci, Part A: Polym Chem. 2002;40:3542-7.

[75] Serizawa T, Wakita K, Akashi M. Rapid deswelling of porous poly(*N*-isopropylacrylamide) hydrogels prepared by incorporation of silica particles. Macromolecules. 2002;35:10-2.

[76] Serizawa T, Wakita K, Kaneko T, Akashi M. Thermoresponsive properties of porous poly(*N*-isopropylacrylamide) hydrogels prepared in the presence of nanosized silica particles and subsequent acid treatment. J Polym Sci, Part A: Polym Chem. 2002;40:4228-35.

[77] Zhang X-Z, Yang Y-Y, Chung T-S, Ma K-X. Preparation and characterization of fast response macroporous poly(*N*-isopropylacrylamide) hydrogels. Langmuir. 2001;17:6094-9.

[78] Kaneko T, Asoh T-A, Akashi M. Ultrarapid molecular release from poly(*N*-isopropylacrylamide) hydrogels perforated using silica nanoparticle networks. Macromol Chem Phys. 2005;206:566-74.

[79] Satarkar NS, Biswal D, ZacháHilt J. Hydrogel nanocomposites: a review of applications as remote controlled biomaterials. Soft Matter. 2010;6:2364-71.

[80] Schexnailder P, Schmidt G. Nanocomposite polymer hydrogels. Colloid Polym Sci. 2009;287:1-11.

[81] Frimpong RA, Fraser S, Zach Hilt J. Synthesis and temperature response analysis of magnetic-hydrogel nanocomposites. J Biomed Mater Res Part A. 2007;80:1-6.

[82] Zhao X, Ding X, Deng Z, Zheng Z, Peng Y, Long X. Thermoswitchable electronic properties of a gold nanoparticle/hydrogel composite. Macromol Rapid Commun. 2005;26:1784-7.

[83] Haraguchi K. Stimuli-responsive nanocomposite gels. Colloid Polym Sci. 2011;289:455-73.

[84] Haraguchi K, Li H-J, Song L. Unusually high hydrophobicity and its changes observed on the newly-created surfaces of PNIPA/clay nanocomposite hydrogels. J Colloid Interface Sci. 2008;326:41-50.

[85] Alzari V, Nuvoli D, Scognamillo S, Piccinini M, Gioffredi E, Malucelli G, et al. Graphene-containing thermoresponsive nanocomposite hydrogels of poly (*N*-isopropylacrylamide) prepared by frontal polymerization. J Mater Chem. 2011;21:8727-33.

[86] Lo C-W, Zhu D, Jiang H. An infrared-light responsive graphene-oxide incorporated poly (N-isopropylacrylamide) hydrogel nanocomposite. Soft Matter. 2011;7:5604-9.

[87] Zhang X, Pint CL, Lee MH, Schubert BE, Jamshidi A, Takei K, et al. Optically-and thermally-responsive programmable materials based on carbon nanotube-hydrogel polymer composites. Nano Letters. 2011;11:3239-44.

[88] Kurihara S, Minagoshi A, Nonaka T. Preparation of poly (*N*-isopropylacrylamide)–$SiO_2$ hybrid gels and their thermosensitive properties. J Appl Polym Sci. 1996;62:153-9.

[89] Hou Y, Fei R, Burkes JC, Lee SD, Munoz-Pinto D, Hahn M, et al. Thermoresponsive nanocomposite hydrogels: transparency, rapid deswelling and cell release. J Biomaterials Tissue Eng. 2011;1:93-100.

[90] Gong JP. Why are double networks so hydrogels so tough? Soft Matter. 2010;6:2583-90.

[91] Gong JP, Kurokawa T, Narita T, Kagata G, Osada Y, Nishimura G, et al. Synthesis of hydrogels with extremely low surface friction. J Am Chem Soc. 2001;123:5582-3.

[92] Gong JP, Katsuyama Y, Kurokawa T, Osada Y. Double-network hydrogels with extremely high mechanical strength. Adv Mater. 2003;15:1155-8.

[93] Myung D, Koh W, Ko J, Hu Y, Carrasco M, Noolandi J, et al. Biomimetic strain hardening in interpenetrating polymer network hydrogels. Polymer. 2007;48:5376-87.

[94] Yasuda K, Gong JP, Katsuyama Y, Nakayama A, Tanabe Y, Kondo E, et al. Biomechanical properties of high-toughness double network hydrogels. Biomaterials. 2005;26:4468-75.

[95] Weng L, Gouldston A, Wu Y, Chen W. Mechanically strong double network photocrosslinked hydrogels from *N*,*N*-dimethylacrylamide and glycidyl methacrylated hyaluronan. Biomaterials. 2008;29:2153-63.

[96] Zhang X-Z, Wu D-Q, Chu C-C. Synthesis, characterization and controlled drug release of thermosensitive IPN-PNIPAAm hydrogels. Biomaterials. 2004;25:3793-805.

[97] Hahn MS, McHale MK, Wang E, Schmedlen RH, West JL. Physiological pulsatile flow bioreactor conditioning of poly(ethylene glycol)-based tissue engineering grafts. Ann Biomed Eng. 2007;35:190-200.

[98] Rathjen CM, Park C-H, Goodrich PR, Walgenbach DD. The effect of preparation temperature on some properties of a temperature-sensitive hydrogel. Polym Gels Networks. 1995;3:101-15.

[99] Kayaman N, Kazan D, Erarslan A, Okay O, Baysal BM. Structure and protein separation efficiency of poly(*N*-isopropylacrylamide) gels: Effect of synthesis conditions. J Appl Polym Sci. 1998;67:805-14.

[100] Shibayama M, Mizutani S-y, Nomura S. Thermal properties of copolymer gels containing *N*-isopropylacrylamide. Macromolecules. 1996;29:2019-24.

[101] Shibayama M, Morimoto M, Nomura S. Phase separation induced mechanical transition of poly(*N*-isopropylacrylamide)/water isochore gels. Macromolecules. 1994;27:5060-6.

[102] Feil H, Bae YH, Feijen J, Kim SW. Effect of comonomer hydrophilicity and ionization on the lower critical solution temperature of *N*-isopropylacrylamide copolymers. Macromolecules. 1993;26:2496-500.

[103] Otake K, Inomata H, Konno M, Saito S. Thermal analysis of the volume phase transition with *N*-isopropylacrylamide gels. Macromolecules. 1990;23:283-9.

[104] Singh D, Knuckling D, Choudhary V, Adler H-J, Koul V. Synthesis and characterization of poly(*N*-isopropylacrylamide) films by photopolymerization. Polym Adv Technol. 2006;17:186-92.

[105] Tanaka Y, Gong JP, Osada Y. Novel hydrogels with excellent mechanical performance. Prog Polym Sci. 2005;30:1-9.

[106] Schild HG. Poly(*N*-isopropylacrylamide): Experiment, theory, and application. Prog Polym Sci. 1992;17:163-249.

[107] Callwaert M, Rouxhet PG, Boulange-Petermann L. Modifying stainless steel surfaces with responsive polymers: effect of PS-PAA and PNIPAAM on cell adheshion and oil removal. J Adhesion Sci Technol. 2005;19:765-81.

[108] Zhang X-Z, Xu X-D, Cheng S-X, Zhuo R-X. Strategies to improve the response rate of thermosensitive PNIPAAm hydrogels. Soft Matter. 2008;4:385-91.

[109] Haraguchi K, Li H-J. Mechanical properties and structure of polymer-clay nanocomposite gels with high clay content. Macromolecules. 2006;39:1898-905.

[110] Yoshida R, Uchida K, Kaneko Y, Sakurai Y, Okano T. Comb-type grafted hydrogels with rapid deswelling response to temperature changes. Nature. 1995;374:240-2.

[111] Xue W, Champ S, Huglin MB, Jones TGJ. Rapid swelling and deswelling in cryogels of crosslinked poly(*N*-isopropylacrylamide-co-acrylic). Eur Polym J. 2004;40:703-12.

[112] Zhang X-Z, Yang Y-Y, Chung T-S. Effect of mixed solvents on characteristics of poly(*N*-isopropylacrylamide) gels. Langmuir. 2002;18:2538-42.

[113] Suthar B, Xiao HX, Klempner D, Frisch KC. A review of kinetic studies on the formation of interpenetrating polymer networks. Polym Adv Tech. 1995;7:221-33.

[114] Haque MA, Kurokawa T, Gong JP. Super tough double network hydrogels and their application as biomaterials. Polymer. 2012;53:1805-22

[115] Kelmanovich SG, Parke-Houben R, Frank CW. Competitive swelling forces and interpolymer complexation in pH- and temperature-sensitive interpenetrating network hydrogels. Soft Matter. 2012;8:8137-48.

[116] Fei R, George JT, Park J, Grunlan MA. Thermoresponsive nanocomposite double network hydrogels. Soft Matter. 2012;8:481-7.

[117] Turan E, Demirci S, Caykara T. Thermo- and pH-induced phase transitions and network parameters of poly(*N*-isopropylacrylamide-*co*-2-acrylamido-2-methyl-propanosulfonic acid) hydrogels. J Polym Sci, Part B: Polym Phys. 2008;46:1713-24.

[118] Travas-Sejdic J, Easteal A. Swelling equilibria and volume phase transition of polyelectrolyte gel with strongly dissociated groups. Polym Gels Networks. 1998;5:481-502.

[119] Melekaslan D, Okay O. Swelling of strong polyelectrolyte hydrogels in polymer solutions: effect of ion pair formation on the polymer collapse. Polymer. 2000;41:5737-47.

[120] Liu X, Tong Z, Hu O. Swelling equilibria of hydrogels with sulfonate groups in water and in aqueous salt solutions. Macromolecules. 1995;28:3813-7.

[121] Okay O, Sariisik SB, Zor SD. Swelling behavior of anionic acrylamide-based hydrogels in aqueous salt solutions: comparison of experiment with theory. J Appl Polym Sci. 1998;70:567-75.

[122] Na Y-H, Kurokawa T, Katsuyama Y, Tsukeshiba H, Gong JP, Osada Y, et al. Structural characteristics of double network gels with extremely high mechanical strength. Macromolecules. 2004;37:5370-4.

[123] Nakajima T, Furukawa H, Gong JP, Lin EK, Wu Wl. A deformation mechanism for double network hydrogels with enhanced toughness. Macromolecular symposia: Wiley Online Library; 2010. p. 122-6.

[124] Travas-Sejdic J, Easteal A. Swelling equilibria and volume phase transition of polyelectrolyte gel with strongly dissociated groups. Polym Gels Networks. 1998;5:481-502.

[125] Singh D, Kuckling D, Choudhary V, Adler HJ, Koul V. Synthesis and characterization of poly (*N*-isopropylacrylamide) films by photopolymerization. Polym Adv Technol. 2006;17:186-92.

[126] Feil H, Bae YH, Feijen J, Kim SW. Effect of comonomer hydrophilicity and ionization on the lower critical solution temperature of *N*-isopropylacrylamide copolymers. Macromolecules. 1993;26:2496-500.

[127] Zhang XZ, Wu DQ, Chu CC. Effect of the crosslinking level on the properties of temperature sensitive poly (*N*-isopropylacrylamide) hydrogels. J Polym Sci, Part B: Polym Phys. 2003;41:582-93.

[128] Bekiari V, Lianos P. Photophysical behavior of terpyridine-lanthanide ion complexes incorporated in a poly(*N*,*N*-dimethylacryalmide) hydrogel. Langmuir. 2006;22:8602-6.

[129] Okay O, Durmaz S. Charge density dependence of elastic modulus of strong polyelectrolyte hydrogels. Polymer. 2002;43:1215-21.

[130] Tong Z, Liu Z. Dynamic mechanical behavior of polyelectrolyte gels with sulfonic acid groups. Macromolecules. 1993;26:4964-6.

[131] Brown HR. A model of the fracture of double network gels. Macromolecules. 2007;40:3815-8.

[132] Yang J, Yamato M, Kohno C, Nishimoto A, Sekine H, Fukai F, et al. Cell sheet engineering: recreating tissues without biodegradable scaffolds. Biomaterials. 2005;26:6415.

[133] Yang J, Yamato M, Shimizu T, Sekine H, Ohashi K, Kanzaki M, et al. Reconstruction of functional tissues with cell sheet engineering. Biomaterials. 2007;28:5033-43.

[134] Gant R, Abraham A, Hou Y, Grunlan MA, Cote GL. Design of a self-cleaning thermoresponsive nanocomposite hydrogel membrane for implantable biosensors. Acta Biomater. 2010;6:2903-010.

[135] Liu W, Zhang B, Lu WW, Li X, Zhu D, Yao KDY, et al. A rapid temperature-responsive sol-gel reversible poly(*N*-isopropylacrylamide)-g-methylcellulose copolymer hydrogel. Biomaterials. 2004;25:3005-12.

[136] Matsuura T, Sugiyama M, Annaka M, Hara Y, Okano T. Microscopic implication of rapid shrinking of comb-type grafted poly(*N*-isopropylacrylamide) hydrogels. Polymer. 2003;44:4405-9.

[137] Kwon OH, Kikuchi A, Yamato M, Sakurai Y, Okano T. Rapid cell sheet detachment from poly(*N*-isopropylacrylamide)-grafted porous cell culture membranes. J Biomed Mater Res. 2000;50:82-9.

[138] Matsuo ES, Tanaka T. Kinetics of discontinuous volume-phase transition of gels. J Chem Phys. 1988;89:1695-703.

[139] Erbil C, Aras S, Uyanik N. Investigation of the effect of type and concentration of ionizable comonomer on the collapse behavior of *N*-isopropylacrylamide copolymer gels in water. J Polym Sci Part A: Polym Chem. 1999;37:1847-55.

[140] Beltran S, Baker JP, Hooper HH, Blanch HW, Prausnitz JM. Swelling equilibria for weakly ionizable, temperature-sensitive hydrogels. Macromolecules. 1991;24:549-51.

[141] Aoyagi T, Ebara M, Sakai K, Sakurai Y, Okano T. Novel bifunctional polymer with reactivity and temperature sensitivity. J Biomater Sci Polym Ed. 2000;11:101-10.

[142] Ebara M, Yamato M, Hirose M, Aoyagi T, Kikuchi A, Sakai K, et al. Copolymerization of 2-carboxyisopropylacrylamide with *N*-isopropylacrylamide accelerates cell detachment from grafted surfaces by reducing temperature. Biomacromolecules. 2003;4:344-9.

[143] Schmaljohann D, Oswald J, Jørgensen B, Nitschke M, Beyerlein D, Werner C. Thermo-responsive PNIPAAm-*g*-PEG films for controlled cell detachment. Biomacromolecules. 2003;4:1733-9.

[144] Weng L, Gouldstone A, Wu Y, Chen W. Mechanically strong double network photocrosslinked hydrogels from *N,N*-dimethylacrylamide and glycidyl methacrylated hyaluronan. Biomaterials. 2008;29:2153-63.

[145] Chandra D, Taylor JA, Yang S. Replica molding of high-aspect-ratio (sub-)micron hydrogel pillar arrays and their stability in air and solvent. Soft Matter. 2008;4:979-84.

[146] Kuckling D, Hoffman J, Plotner M, Ferse D, Kretschmer K, Adler H-JP, et al. Photo cross-linkabe poly(*N*-isopropylacrylamide) copolymers III: micro-fabricated temperature responsive hydrogels. Polymer. 2003;44:4455-62.

[147] Hou H, Hou Y, Grunlan MA, Munoz-Pinto DJ, Hahn MS, Han A. Micropatterning of poly(*N*-isopropylacrylamide) (PNIPAAm) hydrogels: effects of thermosensitivity and cell release behavior. Sensors and Materials. 2010;22:109-20.

[148] Tsai H-T, Vats K, Yates MZ, Benoit DSW. Two-dimensional patterns of poly(*N*-isopropylacrylamide) microgels to spatially control fibroblast adhesion and temperature-responsive detachment. Langmuir. 2013;29:12183-93.

[149] Yamato M, Konno C, Utsumi M, Kikuchi A, Okano T. Thermally responsive polymer-grafted surfaces facilitate patterned cell seeding and co-culture. Biomaterials. 2002;23:561-7.

[150] Tsuda Y, Kikuchi A, Yamato M, Nakao A, Sakurai Y, Umezu M, et al. The use of patterned dual thermoresponsive surfaces for the collective recovery as co-cultured sheets. Biomaterials. 2005;26:1885-93.

[151] Takata S-i, Norisuye T, Shibayama M. Preparation temperature dependence and effects on hydrolysis on static inhomogeneities of poly(acrylamide) gels. Macromolecules. 1999;32:3989-93.

[152] Fei R, George JT, Park J, Grunlan MA. Thermoresponsive nanocomposite double network hydrogels. Soft Matter. 2011;8:481-487.

[153] Fei R, George JT, Park J, Means AK, Grunlan MA. Ultra-strong thermoresponsive double network hydrogels. Soft Matter. 2013;9:2912-9.

[154] Hannoun BJ, Stephanopoulos G. Diffusion coefficients of glucose and ethanol in cell-free and cell-occupied calcium alginate membranes. Biotechnol Bioeng. 1986;28:829-35.

[155] Teixeira J, Mota M, Venâncio A. Model identification and diffusion coefficients determination of glucose and malic acid in calcium alginate membranes. Chem Eng J and Biochem Eng J. 1994;56:B9-B14.

[156] Zhang W, Furusaki S. On the evaluation of diffusivities in gels using the diffusion cell technique. Biochem Eng J. 2001;9:73-82.

[157] Venâncio A, Teixeira J. Characterization of sugar diffusion coefficients in alginate membranes. Biotechnol Tech. 1997;11:183-6.

[158] Khalil E, Kretsos K, Kasting GB. Glucose partition coefficient and diffusivity in the lower skin layers. Pharm Res. 2006;23:1227-34.

[159] Russell R, Axel A, Shields K, Pishko M. Mass transfer in rapidly photopolymerized poly (ethylene glycol) hydrogels used for chemical sensing. Polymer. 2001;42:4893-901.

[160] Tuchin VV. Handbook of optical sensing of glucose in biological fluids and tissues: CRC Press; 2009; p xxxii, 709p.

[161] Aussedat B, Dupire-Angel M, Gifford R, Klein J, Wilson G, Reach G. Interstitial glucose concentration and glycemia: implications for continuous subcutaneous glucose monitoring. Am J Physiol-Endoc M. 2000;278:E716-E28.

[162] Baker DA, Gough DA. Dynamic delay and maximal dynamic error in continuous biosensors. Anal Chem. 1996;68:1292-7.

[163] Heise T, Koschinsky T, Heinemann L, Lodwig V. Hypoglycemia warning signal and glucose sensors: requirements and concepts. Diabetes Technol Ther. 2003;5:563-71.

[164] Rebrin K, Steil GM. Can interstitial glucose assessment replace blood glucose measurements? Diabetes Technol Ther. 2000;2:461-72.

[165] Rebrin K, Steil GM, Van Antwerp WP, Mastrototaro JJ. Subcutaneous glucose predicts plasma glucose independent of insulin: implications for continuous monitoring. Am J Physiol-Endoc M. 1999;277:E561-E71.

[166] Okano T, Yamada N, Okuhara M, Sakai H, Sakurai Y. Mechanism of cell detachment from temperature-modulated, hydrophilic-hydrophobic polymer surfaces. Biomaterials. 1995;16:297-303.

[167] Renner K, Amberger A, Konwalinka G, Kofler R, Gnaiger E. Changes of mitochondrial respiration, mitochondrial content and cell size after induction of apoptosis in leukemia cells. Biochim Biophys Acta. 2003;1642:115-23.